



## UvA-DARE (Digital Academic Repository)

### Bending benzenes and twisting light

Kovida, K.

**Publication date**  
2026

[Link to publication](#)

#### **Citation for published version (APA):**

Kovida, K. (2026). *Bending benzenes and twisting light*. [Thesis, fully internal, Universiteit van Amsterdam].

#### **General rights**

It is not permitted to download or to forward/distribute the text or part of it without the consent of the author(s) and/or copyright holder(s), other than for strictly personal, individual use, unless the work is under an open content license (like Creative Commons).

#### **Disclaimer/Complaints regulations**

If you believe that digital publication of certain material infringes any of your rights or (privacy) interests, please let the Library know, stating your reasons. In case of a legitimate complaint, the Library will make the material inaccessible and/or remove it from the website. Please Ask the Library: <https://uba.uva.nl/en/contact>, or a letter to: Library of the University of Amsterdam, Secretariat, P.O. Box 19185, 1000 GD Amsterdam, The Netherlands. You will be contacted as soon as possible.

# 1

## Introduction

## 1.1 From Hands to Molecules: Brief History of Chirality

Chirality represents one of the most fundamental and ubiquitous properties in nature, describing objects that cannot be superimposed on their mirror images through any combination of rotation and translation. The term itself derives from the Greek word “χειρ” (kheir), meaning hand, reflecting the most familiar example of chiral objects: our left and right hands. The historical journey of chirality as a scientific concept began with serendipitous observations in the mid-19th century and evolved into one of chemistry’s most fundamental principles. The earliest scientific evidence for chirality emerged when Jean Baptiste Biot discovered optical rotation in quartz crystals in 1812, followed by his observations of optical rotation in camphor in 1815.<sup>1</sup>

However, the true breakthrough came in 1848 when Louis Pasteur made his landmark discovery while studying tartaric acid crystals. Pasteur demonstrated that the mirror image crystals of sodium ammonium tartrate rotated linear polarized light in opposite directions. This observation established the fundamental connection between molecular structure and optical activity, revealing that optical rotation was the primary physical property by which chiral molecules could be distinguished.<sup>2</sup> The formal conceptualization of chirality took shape in the late 19th century when Lord Kelvin introduced the term “chirality” in 1894, though it had previously been called “dissymmetry”.<sup>3</sup> Kelvin’s precise definition established the mathematical foundation:

***“I call any geometrical figure, or group of points, ‘chiral’, and say that it has chirality if its image in a plane mirror, ideally realized, cannot be brought to coincide with itself”.***

Further, the historical development of stereochemical understanding profoundly impacted biological sciences, as scientists recognized that the tetravalent carbon center occupies the vertices of a tetrahedron. This geometric insight, developed independently by Le Bel<sup>4</sup> and Van ‘t Hoff<sup>5,6</sup>, became fundamental to understanding molecular structure.<sup>7</sup> As the field matured, the recognition of chiral molecules expanded rapidly across multiple disciplines. The discovery revealed that chiral molecules exist as enantiomers: two spatial isomeric configurations made from the same atoms, where one configuration is the incongruent mirror image of the other. Scientists began to recognize that chirality was not limited to simple carbon-centered molecules but extended to complex biological structures including DNA, proteins, and other essential biomolecules. The pharmaceutical implications of chiral molecule discovery became increasingly important as scientists recognized that while chiral molecules typically share many physical properties such as

density and viscosity, they can demonstrate completely different effects in biology. The tragic case of thalidomide serves as a stark reminder of chirality's importance, where one enantiomer provided therapeutic benefits while its mirror image caused severe birth defects.<sup>8</sup>

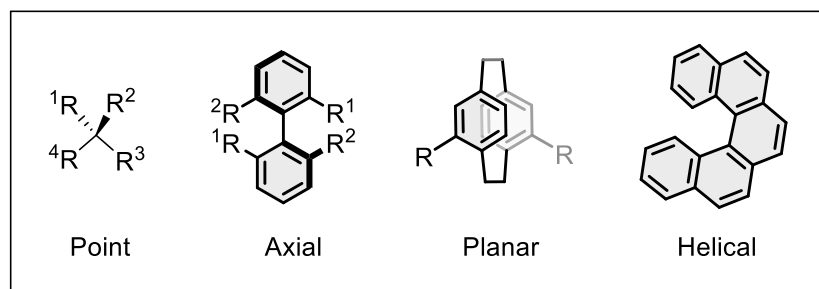


**Figure 1.1.** Classification of chirality based on their dimensional origin.

The concept of chirality is far more diverse than the simple, most familiar case of a single carbon atom bonded to four different groups. To manage this complexity, scientists often classify chiral structures based on their dimensional origin, that is the geometric feature that creates the mirror-image asymmetry (Figure 1.1). The major categories include: (i) **Point (0D) chirality** which is the classical form, arising from a central atom (or point) like a tetrahedral carbon atom (ii) **Axial (1D) chirality**<sup>9</sup> which occurs when restricted rotation creates asymmetry along an axis, causing the molecule to twist as observed in widely used compounds like BINAP (iii) **Planar (2D) chirality**<sup>10</sup> which arises from non-symmetrical arrangements around a flat plane and (iv) **Helical<sup>11</sup> or Supramolecular<sup>12</sup> (3D) chirality** which describes screw-like, spiral structures which are crucial in large systems like the DNA double helix or other complex non-covalent assemblies.<sup>12</sup> Beyond this classification, there are more types of chirality such as topological chirality, found in molecular knots and catenanes,<sup>13</sup> and curvature-induced chirality,<sup>14</sup> which can be observed in large twisted or bowl-shaped molecules.

## 1.2 Fundamentals of Chiroptical Spectroscopy

Light in its ordinary unpolarized state, like the light from the Sun, a lamp or a candle, is fundamentally random in polarization orientation. Its electric field oscillates in different directions simultaneously, perpendicular to the direction of light wave. When this oscillation is somehow constrained or organized, the light becomes polarized. Polarization essentially describes the specific pattern that the light's electric field follows as the wave propagates. Scientists categorize

polarized light based on the shape of this oscillation pattern, the main types include linearly polarized (LP) light, where the oscillation is restricted to a straight line, and circularly polarized (CP) light, which is critical for circularly polarized luminescence (CPL) applications such as advanced display technologies, optical data storage and sensors.<sup>15,16</sup> In CP light, the electric field follows a spiral path as the light moves forward. In this case, two circular polarization states exist. In the left-handed circular polarization state, the propagation of electric and magnetic field vectors describe an anticlockwise helix, while the associated vectors follow a clockwise helix in case of right-handed circular polarization.<sup>17</sup> This circular polarization brings chiral character to photons and constitutes the basis of what we now refer to as “chiroptics” in broad terms.

**Generation of CP light:** There are two primary approaches for generating circularly polarized light, each with their own distinct advantages and limitations. The traditional method relies on external optical equipment. First, ordinary unpolarized light is passed through a linear polarizer to make it linearly polarized followed by a quarter-wave plate which twists the linear polarization into a circular spiral, but this process causes approximately 50% energy loss during the traversing of plates as well as the conversion of unpolarized light into linearly polarized light. This led scientists to the direct generation approach: design of chiral non racemic light-emitting molecules (luminophores) that naturally emit CP light in the form of CPL immediately upon excitation, while avoiding the energy wasting steps of optical plate transitions.

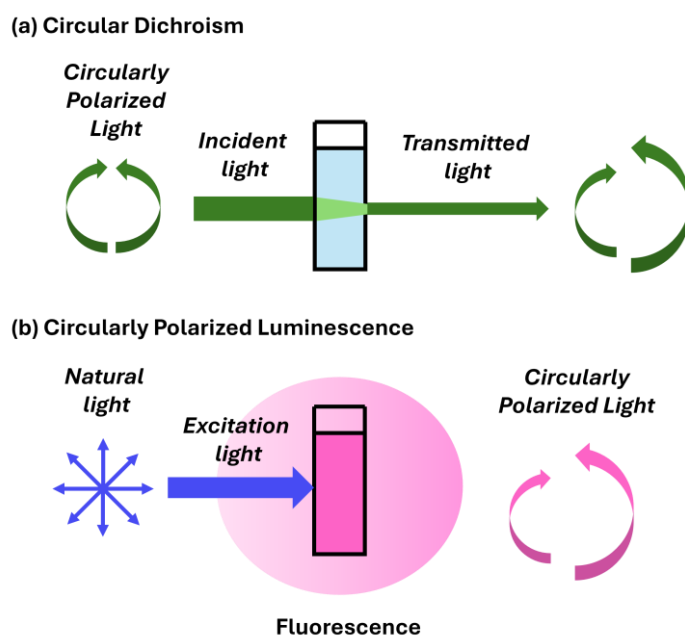


**Figure 1.2.** Difference between CD and CPL. Adapted from Ref.<sup>18</sup>

Chiral molecules interact differently with left-handed circularly polarized (LCP) light and right-handed circularly polarized (RCP) light. This differential interaction manifests in two complementary ways: Circular Dichroism (CD) and CPL (Figure 1.2). **CD** occurs when a chiral molecule preferentially absorbs one handedness of light over the other and is a powerful tool for examining the configuration and shape of structures while they are in their non-excited, relaxed ground state.<sup>19</sup> **CPL** on the other hand occurs when a chiral molecule preferentially emits one handedness of light over the other upon excitation.<sup>20</sup> CPL is unique as it reveals the structure and chirality of the molecule when it is in its energized excited state, just as it is emitting light. In short, CD tells us what the molecule looks like when it's resting, and CPL tells us what it looks like when it's glowing. Therefore, chiral molecules can revolutionize applications in next-generation display technology,<sup>21,22</sup> sensing and bio imaging,<sup>23</sup> anti-counterfeiting,<sup>24</sup> information storage,<sup>25</sup> chiroptical probe,<sup>26</sup> and spintronics<sup>27</sup> etc.

**A brief history of CPL:** CPL was first measured in 1948 by Samoilov<sup>28</sup> on a chiral crystal of sodium uranyl acetate and actively pursued in 1960 by Oosterhoff and co-workers. In fact, the theoretical basis of the CPL technique was established by Emeis and Oosterhoff at the Leiden University.<sup>29</sup> Measurements were performed by manually rotating a quarter wave plate followed by continuous rotation with phase-sensitive detection. The technique was constantly improved by Dekkers and co-workers.<sup>30</sup> A few years later, Steinberg and Gafni developed their own instrument and studied molecules of biological interest.<sup>31</sup> Soon after, many articles have been reported by researchers from different fields.<sup>32-34</sup> The potential of CPL was confirmed in 1980, when Wynberg and co-workers published their findings that the left and right light organs (lanterns) of two firefly species (*Photuris lucicrescens* and *Photuris versicolor*) produce CPL of opposite sense.<sup>35</sup>

**General theory of ECD and CPL:** Among various CD techniques that are classified based on the region of absorbed light, Electronic Circular Dichroism (ECD) technique is widely used due to its high sensitivity and reliability for studying chiral molecules.<sup>36,37</sup> ECD is fundamentally defined as the differential absorption ( $\Delta A$ ) of left-handed and right-handed circularly polarized light (LCP and RCP) by chiral molecules and mathematically expressed as:

$$\Delta A = A_L - A_R \quad (1)$$

where  $A_L$  and  $A_R$  represent the absorption intensities for left and right handed circularly polarized light, respectively. On the other hand, the difference in emission intensity ( $\Delta I$ ) of left-handed ( $I_L$ )

and right-handed ( $I_R$ ) circularly polarized light can be accessed using CPL spectroscopy and is defined as:

$$\Delta I = I_L - I_R \quad (2)$$

Due to the difficulty in measuring the absolute values of emission intensities, the dissymmetry factor,  $g$ , is used which is defined as the ratio of the difference in intensities of left and right handed CPL and the average total intensity of the left and right CPL, thus providing a normalized measure of differential circular emission. It can be expressed by the following formula:

$$g_{lum} = \frac{2(I_L - I_R)}{I_L + I_R} \quad (3)$$

The  $\frac{1}{2}$  factor in this equation is included to make the definition of  $g_{lum}$  consistent with the definition of preferential absorption in ECD, in which the molar absorption coefficient  $\epsilon$  is always defined as an average quantity. The dissymmetry factor of absorption can thus be defined as:

$$g_{abs} = \frac{2(\epsilon_L - \epsilon_R)}{\epsilon_L + \epsilon_R} \quad (4)$$

where  $\epsilon_L$  and  $\epsilon_R$  are the molar absorption coefficients for left and right circularly polarized light. It follows that the values of  $g_{abs}$  and  $g_{lum}$  are ranged between +2 and -2 meaning complete polarization of emitted light and 0 corresponding to an unpolarized beam. Typically, chiral organic molecules or macromolecules display  $|g_{lum}|$  values of  $10^{-3} - 10^{-2}$ .<sup>38-40</sup>

Theoretically,  $g_{lum}$  is related to the electric transition dipole moment ( $\mu$ ) and magnetic transition dipole moment ( $m$ ), as well as the angle  $\theta_{\mu,m}$  between them and can be defined as:

$$g_{lum} = \frac{4|\mu| \cdot |m| \cos \theta}{|\mu|^2 + |m|^2} \quad (5)$$

Because magnetic transition dipole moments are usually smaller than electric transition dipole moments for small organic molecules, the denominator in equation is dominated by the electric dipole term. In most cases, the equation can thus be simplified as:

$$g_{lum} = \frac{4|m| \cos \theta}{|\mu|} \quad (6)$$

**CPL brightness:** It was recently realized that although the luminescence dissymmetry factor,  $g_{\text{lum}}$  serves as the primary factor for quantifying CPL activity, it is alone insufficient for assessing real-world applicability since it only considers the relative imbalance of CP light during the emission. Therefore, it is important to consider the total photon output over which polarization is measured for the sample. To address this limitation, a new parameter was proposed by Zinna et. al.,<sup>40</sup> in 2020, alongside a similar parameter by Mori and co-workers.<sup>41</sup> This parameter is called CPL brightness ( $B_{\text{CPL}}$ ) and is defined as:

$$B_{\text{CPL}} = \varepsilon_{\lambda} \times \phi_{\text{Fl}} \times \frac{|g_{\text{lum}}|}{2} \quad (7)$$

This quantity not only considers the dissymmetry factor  $g_{\text{lum}}$ , but also the molar extinction coefficient ( $\varepsilon_{\lambda}$ ) measured at the excitation wavelength ( $\lambda$ ) and fluorescence quantum yield  $\Phi_{\text{Fl}}$ , providing a better assessment of luminophore suitability for chiroptical applications. It also allows for a direct comparison between molecular systems from different classes.

### 1.3 Limitations and Strategies towards CPL emitters

As seen from equation (6), the ability of a molecule to absorb CP light or emit CPL fundamentally requires the simultaneous presence of both  $\mu$  and  $m$ . The strength of a standard electronic transition is primarily determined by  $\mu$ , which arises from a translation of charge density and follows the selection rule that requires a change in parity of the wavefunctions. Conversely, the magnetic transition dipole moment,  $m$ , originates from a rotation of charge density and is associated with transitions that conserve parity. It is in fact the simultaneous charge translation ( $\mu$ ) and rotation ( $m$ ) that is responsible for creating a helical interaction of light and matter. However, the intrinsic difference in their selection rules creates a critical design challenge. Since dissymmetry factor,  $g$  is proportional to the ratio  $|m|/|\mu|$ , maximizing the chiroptical signal requires to minimize the  $|\mu|$ . However, since the overall emission intensity is directly proportional to  $|\mu|^2$ , the pursuit of high dissymmetry often results in weakly emissive or forbidden transitions. This represents a persistent trade-off in the design of chiral materials: enhancing the dissymmetry factor typically comes to the detriment of overall brightness.

**Chiral ketones** offered an important class of CPL emitters to exploit these transitions. In 1967, Emeis and Oosterhoff<sup>29</sup> described the CPL of chiral cyclic ketones and later by Dekkers<sup>42</sup> (Figure 1.3a). These ketones displayed remarkably high  $|g_{\text{abs}}|$  value of 0.2 attributed to the magnetically allowed carbonyl  $n\text{-}\pi^*$  transition situated at around 400 nm. However, these ketones displayed low quantum efficiency ( $\mu$  forbidden). Furthermore, their  $|g_{\text{lum}}|$  are often considerably lower than  $g_{\text{abs}}$  (0.03 for the same ketone) due to the geometric changes of the C=O bond in the excited state, with molar extinction coefficients reported in the order of  $10^2 \text{ M}^{-1} \text{ cm}^{-1}$ . The resulting brightness factor,  $B_{\text{CPL}}$  ( $5.6 \times 10^{-4} \text{ M}^{-1} \text{ cm}^{-1}$ ) was thus too low for practical application, illustrating the importance of balancing both dissymmetry and quantum efficiency.

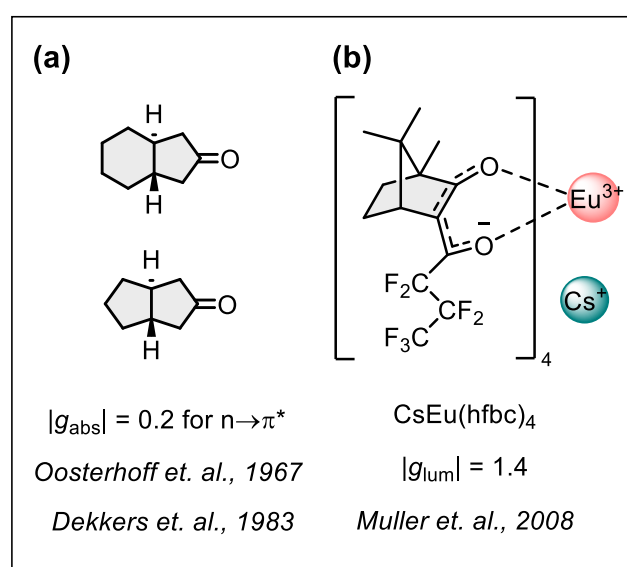


**Figure 1.3.** Chiral ketones and Inorganic complexes as CPL emitters.<sup>29,42,43</sup>

**Inorganic complexes**, particularly those based on lanthanide ions (like Eu (III) and Sm (III)), have emerged with strongest  $g_{\text{lum}}$  values. Lanthanide complexes are characterized by internal Laporte-forbidden  $f\text{-}f$  transitions which are ideal for CPL because they naturally possess large magnetic and weak electric dipole moments. To compensate for the weak absorption, surrounding ligands are strategically employed as antennae. These units efficiently absorb high-energy light and transfer the excitation energy to the lanthanide center in an attempt to improve quantum yield of fluorescence. Record value as high as  $g_{\text{lum}} = 1.38$  has been demonstrated by Muller and co-workers for  ${}^5\text{D}_0 \rightarrow {}^7\text{F}_1$  transition in  $\text{Cs}[\text{Eu}((+)\text{-hfbc})_4]$  complex (Figure 1.3b).<sup>43</sup> Despite their outstanding  $g_{\text{lum}}$ , lanthanide complexes face major challenges. Their emission efficiency is still inherently low (3%) due to the nature of the electronic transitions involved in

the emission. Additionally, their high production costs and the demand for highly purified samples severely limit their practical integration into optoelectronic devices such as CP-OLEDs.

Other **Small organic molecules (SOMs)** including derivatives of cyclophanes, BODIPY, helicenes and pyrene have also been studied as attractive alternatives, largely because they overcome the practical limitations of lanthanide systems.<sup>38,40,44</sup> SOMs offer high emission quantum yields (meaning they waste less energy), easy processing, tunable emission wavelengths, easier structural modification, and have low production costs, making them more suitable for scalable devices. However, SOMs face characteristic challenges such as small  $g_{\text{lum}}$  values which typically fall in the range of  $10^{-5}$  to  $10^{-3}$ . To combat this low dissymmetry, recent research has shifted away from historical models (like the constraint cyclic ketones) towards rigid aromatic systems that possess electronically allowed  $\pi-\pi^*$  transitions. These rigid frameworks provide improved quantum yields, facile structural modification, and systematic excited-state relaxing behavior.

**Engineering dipole moments:** an alternative strategy to engineer the structure of CPL emitter is to achieve a balance between electric and magnetic transition dipole moment vectors and to optimize the angle between them. In this section, only relevant examples of high-performing CPL emitters in the context of complex  $\pi$ -conjugated systems, focused on cyclic conjugated macrocycles will be presented to lay the foundation of the thesis.

In 2018, Mori and co-workers demonstrated that the double hexahelicene (Figure 1.4a), featuring an X-shaped structure, achieved around two-fold enhancement in the chiroptical response compared to the monomeric hexahelicene.<sup>45</sup> This enhancement is mechanistically traced to the high  $D_2$  symmetry of the doublehelicene. This symmetrical configuration resulted in parallel alignment ( $\theta = 0$ ) of  $\mu$  and  $m$ , maximizing the  $\cos \theta$  up to 1 and thus a higher  $g_{\text{lum}}$  value of  $2.5 \times 10^{-3}$  for double helicene relative to hexahelicene ( $g_{\text{lum}} = 0.9 \times 10^{-3}$ ). The authors also discussed the importance of fusing the rings together instead of simply embedding it to achieve better transition dipole moments alignment. The 2020 work by Matsuda and co-workers further emphasized the importance of alignment of the transition dipole moments to reach a favorable angle to improve the chiroptical performance. The authors demonstrated that a figure-eight-shaped helicene dimer with  $D_2$  symmetry exhibits notably high CPL response, achieving a high  $|g_{\text{lum}}|$  of  $1.5 \times 10^{-2}$  (Figure 1.4b). The key to this enhanced CPL lies in the parallel arrangement of electric and magnetic transition dipole moments, as well as a good  $|\mu|/|m|$  ratio.

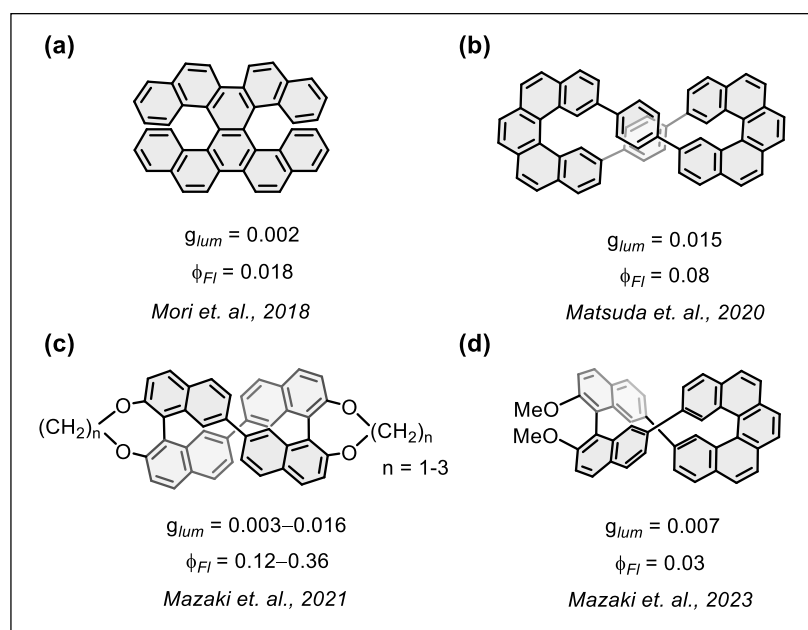


**Figure 1.4.** Chiral  $\pi$ -conjugated systems.<sup>45–48</sup>

**Locking the geometry:** Mazaki and co-workers focused on designing constrained chiral  $\pi$ -systems by creating tethered cyclic binaphthyls and locked helicenes. In the binaphthyl system (Figure 1.4c), they synthesized luminophores in which a short tether forced a highly constrained geometry, achieving remarkable  $g_{lum}$  up to  $1.6 \times 10^{-2}$  by promoting extensive transannular  $\pi$ -core delocalization.<sup>46</sup> Their research into helicene hinged binaphthyl showed that tethering systems could be used to lock the helical conformation, imparting configurational stability and boosting the CPL activity beyond that of their untethered counterparts (Figure 1.4d).<sup>47</sup> Together, this provides a successful method to leverage conformational restriction to precisely align the transition dipole moments.

**Symmetry effects and dissociation of  $g_{lum}/\Phi_{Fl}$  trade-off:** In 2017, Sato, Isobe and co-workers investigated cyclic chrysene oligomers (Figure 1.5) as structural mimics for chiral fragments of single-walled carbon nanotube sidewalls (SWCNT). These macrocycles adopt a three-dimensional cylinder-shaped architecture, achieving maximum point groups of  $D_4$  and  $C_2$ , for **(P)-(12,8)-[4]CC** and **(P)-(11,9)-[4]CC**, respectively, based on the orientation of the dihexyl chrysene units. The resulting highly symmetrical structures conferred exceptionally high  $g_{abs}$  of 0.167 for **(P)-(12,8)-[4]CC**, which can be attributed to the electronic structure, where the MO was delocalized across the entire  $\pi$ -conjugated cylinder. Also, the vector sum of local electric transition dipole

moments ( $\mu$ ) cancelled in the xy plane, resulting in overall  $m$  to be substantially extended along the z-axis, leading to observed  $g_{\text{abs}}$  values.

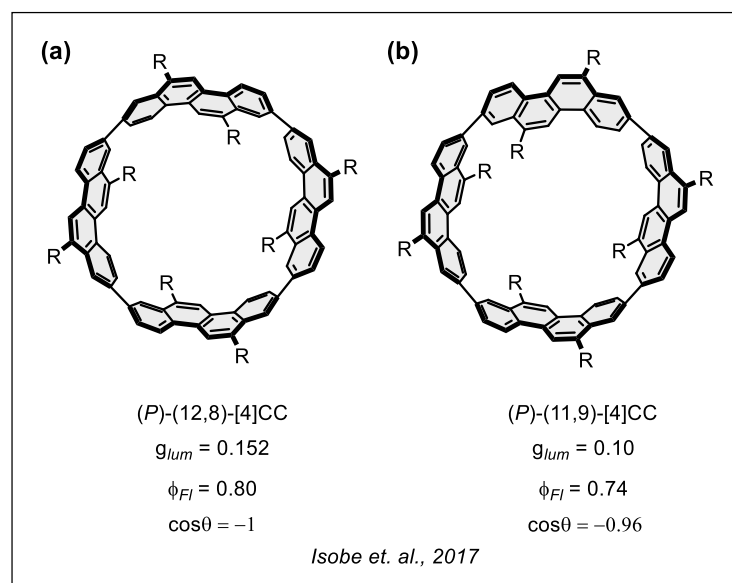


**Figure 1.5.** Chiral cylindrical molecules by Isobe.<sup>49</sup>

Notably, **(P)-(12,8)-[4]CC** exhibited highest reported CPL performance for SOMs, achieving a high  $g_{\text{lum}}$  of 0.152 and a high  $\Phi_{\text{FI}}$  of 0.80 in toluene. These findings are significant because they seemingly decouple the typical trade-off between the dissymmetry factor and quantum yield, a compromise often imposed by the Laporte selection rule. The experimental evidence strongly suggests that the highly symmetrical chiral cylinder structure effectively preserves a large  $m$  vector and favorable angle between the transition dipole moments even in the excited state, offering a strategy for designing high-performance CPL emitters.

Other strategies that employ chromophore coupling, aggregation, self-assembly for enhancing CPL, have also been investigated extensively over the years.

## 1.4 Carbon Nanohoops

Within this diverse family of  $\pi$ -conjugated macrocycles, a particularly intriguing subfamily emerged that captured the imagination of chemists worldwide, namely, **Cycloparaphenylenes** ([n]CPPs), where n represents the number of phenylene rings. These remarkable molecules are tube-shaped radially  $\pi$ -conjugated molecular loops comprised of distorted para-linked phenylene rings. This unique architectural feature gives them their distinctive properties and their evocative nickname: **Carbon Nanohoops**.

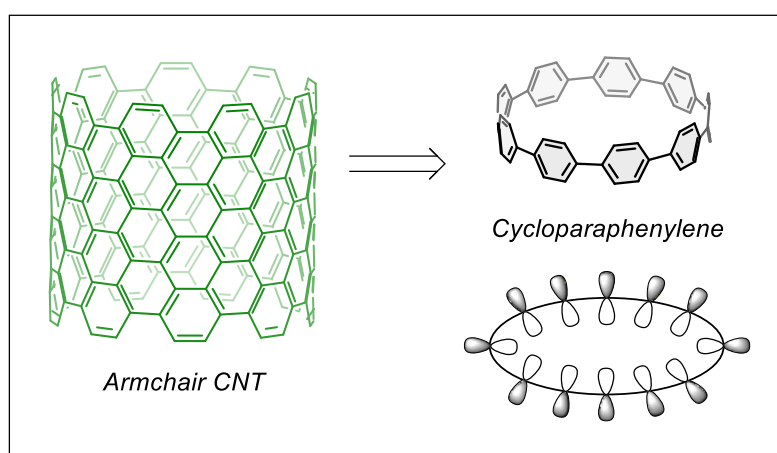


**Figure 1.6.** Cut-off from a carbon nanotube and radial conjugation in CPP.

The structural beauty of CPPs lies in their relationship to one of the most studied materials in nanotechnology. These molecules represent the shortest segments of armchair carbon nanotubes (CNTs),<sup>50</sup> essentially providing chemists with discrete, well-defined molecular models of these extended materials (Figure 1.6). Therefore, carbon nanohoops are ideal models for investigating curvature-induced strain, aromaticity, size-dependent optoelectronic properties, and host-guest interactions.

The quest to synthesize cycloparaphenylenes had tantalized chemists for years before success was finally achieved. Early attempts in 1993 by Vögtle and co-workers laid the groundwork.<sup>51</sup> Although the group was unsuccessful with the synthesis of CPPs, the strategy ultimately helped scientists many years later in achieving the CPPs. First, Vögtle attempted the synthesis of larger [6] and [8]CPPs via desulfurization route (Figure 1.7a) but unfortunately all attempts were unsuccessful. The group also tried to access CPPs using Diels-Alder reactions to install aromatic rings in an existing macrocycle albeit with no success (Figure 1.7b). Third attempt involved

assembling the macrocycles containing cyclohexane rings and arenes as shown in (Figure 1.7c). Such macrocycles were expected to be far less strained than CPPs as they contain  $sp^3$  hybridized carbons which would better accommodate the curvature of the macrocycle. The formed macrocycles could be subsequently aromatized to obtain CPPs, while the increase in strain energy would be compensated by the gain in aromatic stability. However, the macrocyclization of this bent block only resulted in linear oligomers. Nevertheless, these strategies laid the foundation for the successful synthesis of  $[n]$ CPPs two decades later.

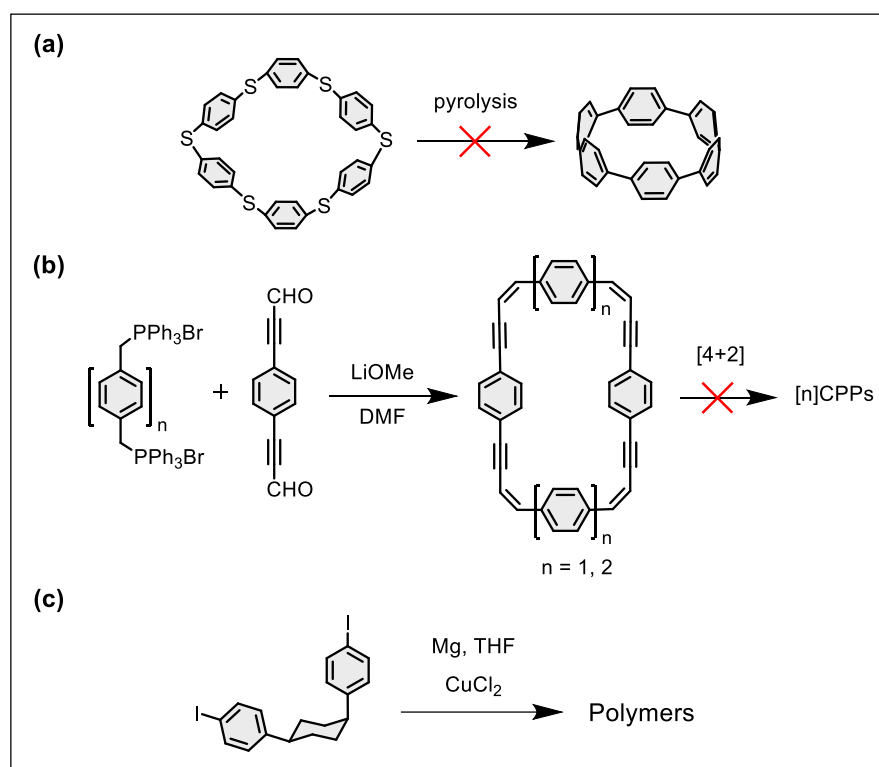


**Figure 1.7.** Early attempts to cycloparaphenylene synthesis by Vögtle.<sup>51</sup>

**The First Synthesis:** In 2008, Jasti, Bertozzi and co-workers achieved what many had thought impossible: the first synthesis of  $[9]$ CPP,  $[12]$ CPP and  $[18]$ CPP (Figure 1.8).<sup>52</sup> The approach is conceptually similar to Vögtle's approach (Figure 1.7c) to CPP synthesis and employs one common precursor for the synthesis of three reported CPPs. A key difference in the synthetic strategy was the use of cyclohexa-1,4-diene instead of cyclohexanes as masked aromatic rings in the CPP precursors. This results in two  $sp^3$  and four  $sp^2$  carbon centers in the masked aromatic unit. This clever approach allowed them to build up strain sequentially during synthesis, with the cyclohexadiene units providing the necessary curvature, rigidity and preorganization for macrocyclization while keeping the strain manageable until the final aromatization step.

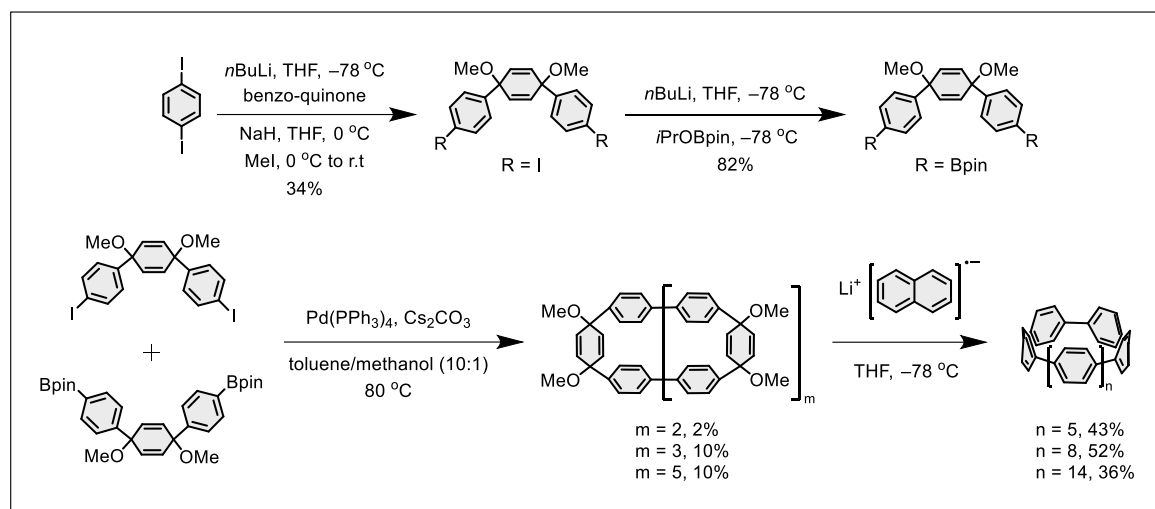


**Figure 1.8.** Synthesis of cycloparaphenylenes ([n]CPPs) by Jasti in 2008.<sup>52</sup>

The synthesis began with monolithiation of diiodobenzene followed by addition of benzoquinone to generate a diol, which was then alkylated with methyl iodide to produce the key diiodide intermediate (Figure 1.8). The diiodide was converted to the corresponding bis(pinacolborane) building block. The authors then attempted macrocyclization using 1:1 mixture of the two difunctionalized precursors under Suzuki-Miyaura cross-coupling conditions. A direct 1:1 adduct of the two precursors would form *pro*-[6]CPP (a precursor to [6]CPP), however no such precursor was observed, but only higher oligomers were formed. Two macrocyclic precursors corresponding to 2:2 adduct and 3:3 adduct were isolated in 10% yield each alongside a smaller unexpected macrocycle. The final reductive aromatization step was performed via single electron transfer reduction using lithium naphthalenide affording the three [n]CPPs in good yields. The authors further measured the absorption and emission spectra of the CPPs and found some surprising results. The absorption maxima were situated at  $\lambda_{\text{max}} \sim 340\text{ nm}$  for all nanohoops irrespective of the ring size. Additionally, an increase in Stokes shift was observed with decrease in ring size. The photophysical properties of [n]CPPs is discussed in detail in later sections.

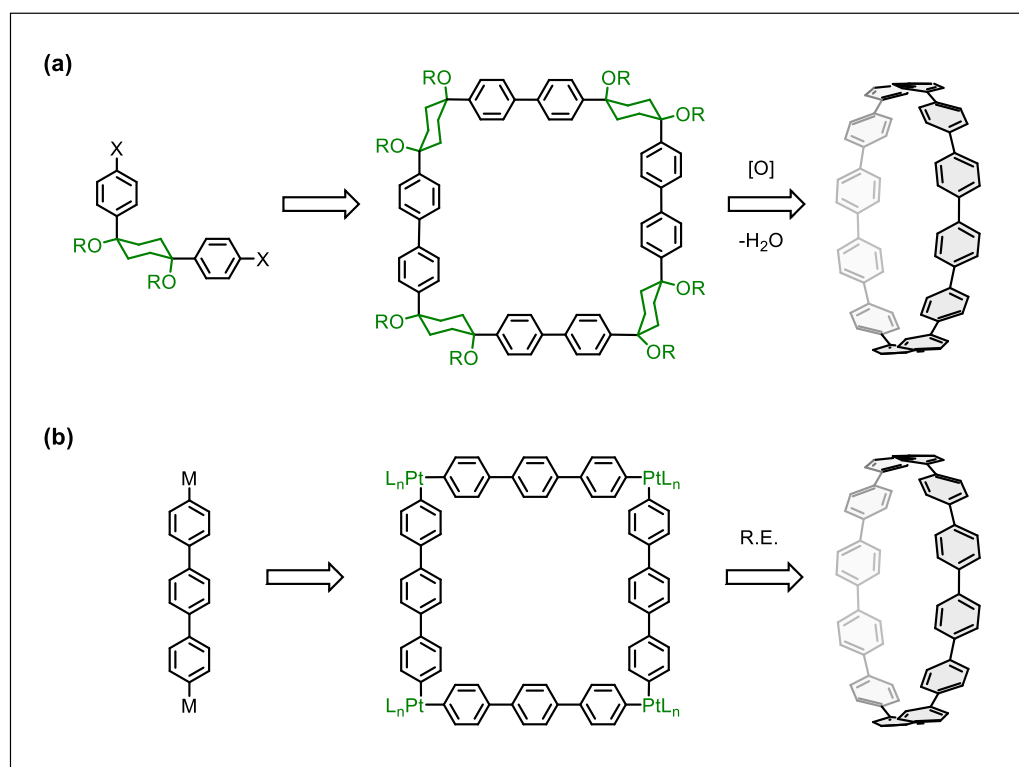


**Figure 1.9.** Synthetic strategies towards CPPs by (a) Itami<sup>53</sup> and (b) Yamago<sup>54</sup> groups.

**Different strategies towards nanohoops:** The 2008 breakthrough opened the floodgates for rapid developments in the field. Soon after, two more synthetic cornerstones were established by the groups of Itami<sup>53</sup> and Yamago,<sup>54</sup> each contributing their own innovative approaches towards nanohoop synthesis. Itami's strategy, which is conceptually based on one of Vögtle's approaches, accesses CPPs through macrocyclization of a precursor containing non-aromatic units, followed by oxidative aromatization step (Figure 1.9a). Their modular synthesis achieved remarkable selectivity in macrocycle construction, leading exclusively to the formation of [12]CPP without producing any other size of cyclic paraphenylene precursor. In 2010, Yamago and co-workers reported another impressive route towards CPPs.<sup>54</sup> Their strategy involves formation of a tetraplatinum precursor to CPP, which is strain free due to the square planar geometry of Pt(II) (Figure 1.9b). Treatment with an oxidant resulted in four-fold reductive elimination to afford the [8]CPP, which was the smallest CPP reported at the time.

## 1.5 Photophysics of Carbon Nanohoops

The photophysical landscape of cycloparaphenylenes does reveal a fascinating interplay between strain, geometry and symmetry that sets them apart from conventional conjugated molecules.<sup>55–57</sup>

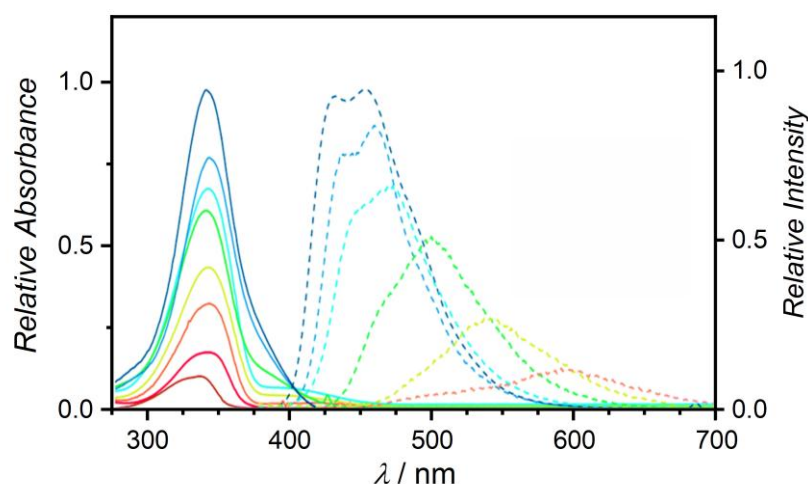
**Table 1.1.** Photophysical properties and Strain energies for [n]CPPs.<sup>55,57–59</sup>

[n]CPP	$\lambda_{\text{abs}} / \text{nm}$	$\lambda_{\text{em}} / \text{nm}$	$\Phi_{\text{FI}}$	Strain / kcal mol <sup>-1</sup>
5	335	-	-	119
6	340	-	-	96.0
7	340	587	0.007	84.0
8	340	533	0.084	72.2
9	340	494	0.30	65.6
10	338	466	0.46	57.7
11	340	458	0.52	53.7
12	339	450	0.66	48.1
13	337	446	0.72	45.5
14	338	443	0.89	41.0
15	339	440	0.90	39.2
16	339	438	0.88	35.6

[n]CPPs exhibit a common size-independent absorption maximum at around 340 nm (Table 1.1).<sup>55,57</sup> The HOMO and LUMO in [n]CPPs are delocalized over all the phenylenes in a centrosymmetric fashion. Therefore, the HOMO–LUMO optical transition in [n]CPPs is symmetry forbidden according to Laporte rule. Calculations also revealed that the HOMO–LUMO transition for even numbered CPPs has an oscillator strength of zero and for odd numbered CPPs it is non-zero due to the inherent low symmetry, however the intensity is still very low. It is observed that [5]–[12]CPPs have degenerate HOMO–1/HOMO–2 and nearly degenerate LUMO+1/LUMO+2. These orbitals have different symmetries than the HOMO and LUMO and the transitions from HOMO–1 or HOMO–2 to LUMO are therefore allowed. Similarly, transition from HOMO to LUMO+1 or LUMO+2 are also allowed resulting in the independent absorption at around 340 nm.<sup>59</sup>

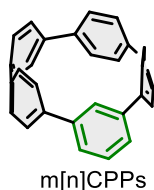
Interestingly, the emission in [n]CPPs is size-dependent with a red-shift in emission observed as the nanohoop size decreases. However, fluorescence quantum yields also decrease with decreasing nanohoop size (Table 1.1, Figure 1.10). For example, [5]CPP and [6]CPP are non-emissive in nature. Many theoretical studies have attempted to explain this observation.<sup>58–65</sup> Calculations show that the populated excited states  $S_2$  and  $S_3$  relax to a geometrically relaxed  $S_1'$  state via fast internal conversion. In larger [n]CPPs ( $n \geq 7$ ) the  $S_1'$  state breaks the symmetry of the

$S_0$  ground state due to exciton localization over seven phenylenes, causing emission to the  $S_0$  state with decreasing quantum yield and red-shifted emission from [12]CPP to [7]CPP. However, in smaller [n]CPPs ( $n \leq 6$ ), the  $S_{1'}$  state conserves the symmetry of the  $S_0$  ground state and emission to the  $S_0$  state is thus symmetry-forbidden and no fluorescence is observed for these smaller CPPs.<sup>60</sup>



**Figure 1.10.** Absorption (solid lines) and emission (dashed lines) spectra of [n]CPPs ( $n=5-12$ ). Adapted from ref.<sup>55</sup>

**Strain energy** of the nanohoops increases dramatically as the nanohoops become smaller. [12]CPP has strain energy of  $48 \text{ kcal mol}^{-1}$  (approximately  $4 \text{ kcal mol}^{-1}$  per aryl ring) while [5]CPP has an estimated  $119 \text{ kcal mol}^{-1}$  of strain energy spread out over only five aryl rings. This equates to be around  $24 \text{ kcal mol}^{-1}$  of strain energy per benzene ring. As the nanohoop size decreases, torsional angles between phenylene rings become smaller to compensate for the increased strain. The decrease in angles leads to a better  $\pi$  overlap and an effective increase in the conjugation between neighboring aryl rings for smaller nanohoops. This also explains the observed narrowing of the HOMO–LUMO energy gap as the number of benzene rings decreases. This is in contrast to linear paraphenylenes, where an increase in the number of aromatic units typically leads to a smaller HOMO–LUMO gap.<sup>66,67</sup> Remarkably, [n]CPPs possess smaller energy gaps than even the longest linear paraphenylenes. Even though smallest CPPs are non-emissive, symmetry breaking in these [n]CPPs can effectively increase the quantum yields and make them emit. This was proven by Jasti et. al., by synthesizing a series of [n]CPPs where one of the phenylene unit is connected via *meta*- position instead of classic *para*- position.<sup>68</sup> The resulting meta cycloparaphenylenes, m[n]CPPs, display fluorescence with improved quantum yields even for smallest rings (Table 1.2).

**Table 1.2.** Photophysical properties and Strain energies of m[n]CPPs.<sup>68</sup>

m[n]CPP	$\lambda_{\text{abs}} / \text{nm}$	$\lambda_{\text{em}} / \text{nm}$	$\Phi_{\text{FI}}$	Strain / kcal mol <sup>-1</sup>
5	316, 428	534	0.01	102
6	328, 410	510	0.22	77.6
7	328, 394	491	0.45	66.4
8	326, 376	484	0.60	56.7
10	328	456	0.73	51.4
12	328	429	0.77	43.3

## 1.6 Going Towards NIR

Over the years, much work has been done to manipulate not only the curvature and size but also the energies of frontier molecular orbitals in carbon nano hoops. For example, a strategy to red-shift the emission in nano hoops was to develop donor–acceptor (D–A)-type [n]CPPs which also have potential applications in optoelectronic devices, such as organic solar cells, OLEDs and sensors etc.<sup>69</sup> Since CPPs have higher HOMO energies than linear paraphenylenes due to the bent  $\pi$ -system, they can be regarded as electron donors. Incorporation of donors such as thiophene into a CPP does not significantly perturb the electronic structure of the nano hoop. Incorporation of acceptors in CPPs on the other hand have shown to lower the LUMO energy and cause bathochromic shifts. Incorporating both donors and acceptors into the CPP framework at the same time, results in D–A system where HOMO localizes on the donor and LUMO localizes on the acceptor moiety. This results in lowering of the HOMO–LUMO gap. A theoretical prediction of optical properties based on donor and acceptor placement was thoroughly investigated by Jasti et. al. using calculations,<sup>70</sup> with predicted emission for some models reaching near-infrared (NIR) region.

In 2015, Itami and co-workers reported the first D–A nano hoop by introducing anthraquinone as an acceptor into [10]CPP as the donor (Figure 1.11a).<sup>71</sup> The acceptor character was further increased by transforming the anthraquinone motif into a tetracyanoanthraquinodimethane group. The absorption maxima for both nano hoops were identical to the parent [12]CPP. **[10]CPAq** exhibits green fluorescence in CCl<sub>4</sub> ( $\lambda_{\text{max}} = 496 \text{ nm}$ ) with emission red-shifted to orange ( $\lambda_{\text{max}} = 591 \text{ nm}$ ) in more polar chlorobenzene. **[10]CPTcaq** displays a red fluorescence in CCl<sub>4</sub> but was non-emissive in polar solvents. In the same year, Jasti et. al. reported nitrogen-containing variants (Aza-[8]CPPs, Figure 1.11b) via incorporation of pyridinium moieties as acceptors.<sup>72</sup> They demonstrate slight red-shifts in their major absorption peaks, with CPP derivatives showing absorption maxima at 345 nm ( $\epsilon = 2.5 \times 10^5 \text{ M}^{-1} \text{ cm}^{-1}$ ), 349 nm ( $\epsilon = 7.3 \times 10^5 \text{ M}^{-1} \text{ cm}^{-1}$ ) and 353

nm ( $\varepsilon = 8.94 \times 10^5 \text{ M}^{-1} \text{ cm}^{-1}$ ) as nitrogen content increases. Further, the nano hoops were methylated using methyl triflate increasing the acceptor character of the pyridine units. This shifts the emission to 598 nm and 630 nm relative to the [8]CPP ( $\lambda_{\text{max}} = 533 \text{ nm}$ ) and the non-methylated versions ( $\lambda_{\text{max}} \sim 542 \text{ nm}$ ).

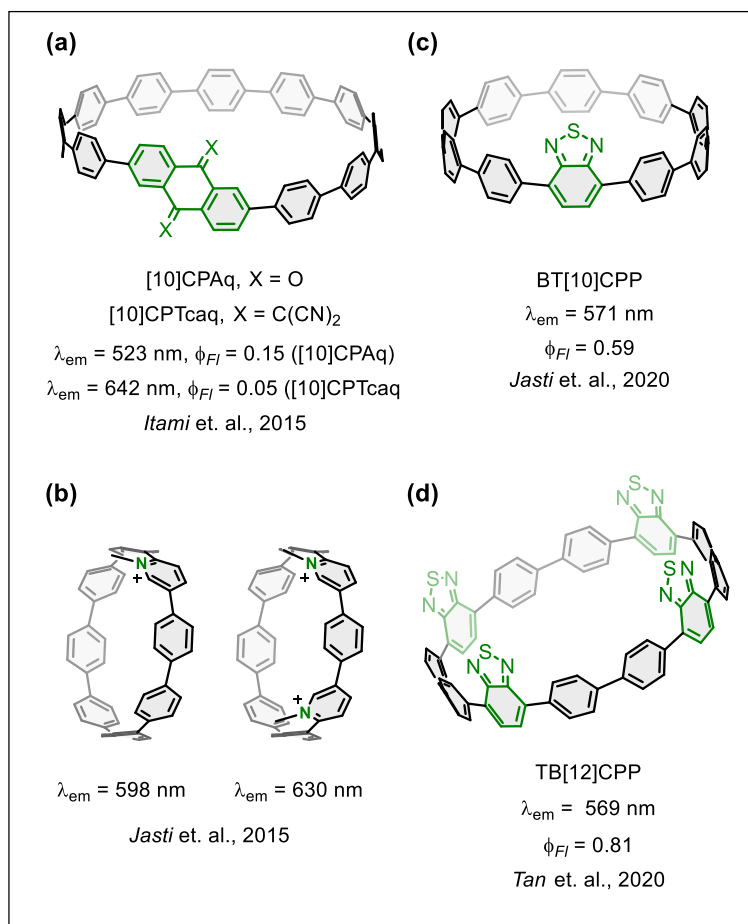


**Figure 1.11.** Donor–Acceptor (D–A) type carbon nano hoops.<sup>71–74</sup>

In 2020, Jasti group reported the first bright-orange emitting benzothiadiazole (BTD)-containing nano hoop, **BT[10]CPP** (Figure 1.11c).<sup>73</sup> While absorption at 334 nm was similar to [10]CPP absorption at 341 nm, the emission maximum was red-shifted by 105 nm to 571 nm owing to the acceptor incorporation. Remarkably, the quantum yield of fluorescence remained high ( $\Phi_{\text{FI}} = 0.59$ ), similar to [10]CPP ( $\Phi_{\text{FI}} = 0.65$ ) which is in contrast to previously reported D–A nano hoops.<sup>73</sup> In the same year, Tan et. al., obtained benzothiadiazole containing nano hoop **TB[12]CPP** (Figure 1.11d) with four BTD groups embedded in the nano hoop.<sup>74</sup> For this nano hoop, two absorption maxima were observed at 320 and 428 nm in CHCl<sub>3</sub>. Introduction of BTD groups red-shifts the absorption of **TB[12]CPP** by 89 nm relative to [12]CPP. The emission

maximum sits at 569 nm (CHCl<sub>3</sub>), markedly red-shifted compared to [12]CPP (450 nm) and displayed positive solvatochromism due to D–A nature. The nano hoop shows a high quantum yield of  $\Phi_{\text{Fl}} = 0.82$  in CHCl<sub>3</sub> solution which further improved to 0.98 in a polymer matrix. Although incorporation of BTD groups resulted in a bright red-shifted emission for the nano hoops discussed above, it is usually difficult to achieve red or NIR emission while maintaining a high fluorescence quantum yields.

Other donor and acceptor containing nano hoops have also been reported in the past decade incorporating acceptors like sulfone,<sup>75</sup> indenofluorenedione,<sup>76</sup> and perylene diimide which was applied as an n-type semiconductor in organic electronic devices.<sup>77</sup> Similarly, introduction of multiple donor groups such as thiophene,<sup>78,79</sup> furans<sup>80</sup> and carbazoles<sup>81,82</sup> were also reported. In 2019, Poriel group reported applications of carbazole containing nano hoops in organic field-effect transistors.<sup>83</sup> Further discussion on acceptor incorporation in carbon nano hoops is presented in subsequent chapters of this thesis.

## 1.7 Synthetic Challenges towards Carbon Nano hoops

The synthesis of carbon nano hoops, while no longer impossible, continues to face fundamental limitations that constrain both the scope and efficiency of synthetic approaches.

**Low Yields:** [n]CPPs synthesis is plagued by consistently low yields severely limiting the accessibility and scale up. Even the pioneering synthetic route developed by Jasti and co-workers, suffers from modest yields at the crucial macrocyclization step using standard Suzuki cross-coupling affording macrocycles in only 22% overall yield even after optimization of conditions. Macrocyclization towards synthesis of [9]cyclonaphthylene nanoring by Itami et. al., for example, only yields the macrocycle in 2% yield.<sup>84,85</sup> The subsequent aromatization of the *pro*-aromatic macrocycles presents additional complications, as cyclohexadiene compounds tend to undergo unwanted rearrangements under acidic conditions and often leads to complex mixtures rather than clean products. These problems become more severe in the synthesis of related carbon nanobelts, which are closely related to CPPs. Their synthesis exhibits poor efficiency with the belt-forming nickel-mediated reaction improved from a dismal 1% to only 7% yield even after optimization with new ligand systems.<sup>86</sup>

**Protection chemistry:** The inherent instability of the precursors and intermediates creates another challenge. The cyclohexadienyl units, commonly employed, contain tertiary alcohols that must be protected prior to the final aromatization step. Protective groups commonly used in CPP synthesis often create their own stability problems that can derail synthetic routes. For example, triethylsilyl (TES) groups, are highly sensitive to acids and compromise the stability of compounds containing them, leading to decomposition during purification or even when stored at low temperatures.<sup>87</sup> The removal of protective groups such as Methoxy (OMe) during aromatization often requires harsh reagents such as sodium naphthalide that can cause unwanted side reactions. However, OMe groups are the most commonly used protecting groups reported so far.

**Post Synthetic Modification:** The ability to perform post-synthetic modification on [n]CPPs is severely restricted by their inherent strain. Upon exposure to standard electrophilic aromatic substitution conditions or Scholl reaction conditions, CPPs undergo facile strain-relieving rearrangements and ring-openings leading to insoluble linear oligomers instead of intended bond-forming reactions.<sup>88</sup> More research on post-synthetic modification of carbon nanohoops is discussed in Chapter 6.

**Chiral Resolution:** Accessing enantiopure samples of chiral carbon nanohoops is important for certain applications such as asymmetric catalysis and chiroptical devices. Currently, the only viable method for obtaining enantiomerically pure carbon nanohoops is through preparative chiral HPLC, which suffers from high costs and scalability. This time-sensitive approach requires multiple chromatographic runs or recycling modes using expensive chiral stationary phases, ultimately allowing isolation of only small quantities of enantiopure nanohoops. In 2021, Esser group presented the first report on conjugated nanohoops, where enantiomers were separated by chiral derivatization of a functionalized nanohoop.<sup>89</sup> There is therefore, a clear research gap and a pressing need for development of new, efficient and scalable methods to achieve the stereoselective synthesis of chiral carbon nanohoops.

## 1.8 Inducing Chirality in Cycloparaphenylenes

Although parent  $[n]$ CPPs are achiral, twisting the phenylenes along the CPP backbone results in a helical structure possessing chiroptical properties. For example, inserting an acene unit into a CPP structure creates helical chirality, however, such structures are configurationally not stable due to rapid rotation of phenylenes around their single C–C bonds. This was demonstrated in 2011 work by Itami and co-workers where the incorporation of achiral naphthalene in CPP backbone results in cyclo[13]paraphenylene-2,6-naphthylene (**[13]CPPN**) which serves as one of the first examples of chiral carbon nanohoops (Figure 1.12a).<sup>90</sup>

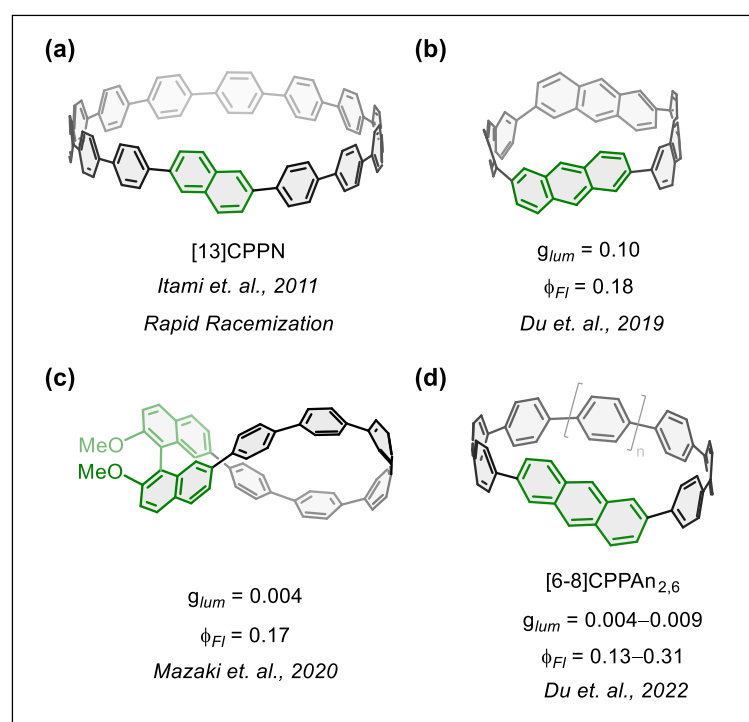


**Figure 1.12.** Structures of chiral carbon nanohoops.<sup>90–93</sup>

The racemization barrier for the synthesized nano hoop was calculated to be  $8.4 \text{ kcal mol}^{-1}$  indicating a rapid racemization at ambient temperature, thereby preventing further chiroptical investigations. Authors further estimated the racemization barriers of other chiral nanohoops namely, CPP-2,6-anthrylene (**[n]CPPA**) and CPP-2,8-tetracenylenes (**[n]CPPT**) to study the effect of ring size and acene units. It was found that the  $\Delta G^\ddagger$  values increase with decreasing ring size and as acene unit becomes larger.<sup>90</sup> More research on racemization of carbon nanohoops is presented in Chapter 5 of this thesis.

An example by Du and co-workers includes the synthesis of anthracene-based conjugated chiral macrocycles, (-)/(+)-[4]cyclo-2,6-anthracene (**[4]CAn<sub>2,6</sub>**) serving as the shortest sidewall segments of chiral (12,4)-SWNTs (Figure 1.12b).<sup>91</sup> These tubular structures demonstrate large absorption and photoluminescence redshifts compared to monomer units and exhibit a strong CPL with relatively high  $g_{\text{lum}}$  values of 0.1, one of the highest reported values for carbon nanostructures in the literature to date. In 2022, the authors extended their work with the synthesis of a series of anthracene-based chiral nanostructures **[n]CPPAn<sub>2,6</sub>**, (n=6-8) with dissymmetry factors measured experimentally for **[6]CPPAn<sub>2,6</sub>** and **[7]CPPAn<sub>2,6</sub>**, which were between  $4.4\text{--}9.1 \times 10^{-3}$  (Figure 1.12d). Emission studies showed a clear red-shift with decreasing size of the **[n]CPPAn<sub>2,6</sub>** with quantum yields ranging from 31 % for **[8]CPPAn<sub>2,6</sub>** to 13% for **[6]CPPAn<sub>2,6</sub>**.<sup>92</sup>

Several chiral nanostructures have been synthesized by incorporating a chiral element into the curved cycloparaphenylene structure to induce a chiral perturbation. Helically curved carbon nanostructures prepared by Mazaki and co-workers is one of many examples (Figure 1.12c).<sup>93</sup> The curved paraphenylenes were twisted by incorporating a chiral binaphthyl unit providing *M* and *P* helicities in the nanostructure. The nanostructure exhibits an intense green emission in solution, powder and PMMA film. Comparable quantum yields of  $\Phi_{\text{fl}} = 0.15\text{--}0.17$  were reported for the nanostructure in solid-state and solution, while an improvement ( $\Phi_{\text{fl}} = 0.47$ ) was observed for the PMMA film due to suppression of molecular motion. This molecule can thus serve as a solid-state CPL dye. The  $|g_{\text{lum}}|$  values of the nanostructure were found to be between  $4.3\text{--}4.4 \times 10^{-3}$  for the solution and PMMA film samples and higher than in the solid-state ( $1.5 \times 10^{-3}$ ). The structure optimization in the excited state by TD-DFT calculations provided a structure with a greater (tight) curvature in the paraphenylenes part of the nanostructure as compared to the ground state. Additionally, the molecular  $\pi$  and  $\pi^*$  orbitals are primarily spread across the curved paraphenylene part thus allowing the exciton to become delocalized. Consequently, a large magnetic transition dipole moment could be produced in the excited state and therefore allow for moderately high  $g_{\text{lum}}$  values.

Another elegant approach to chiral carbon nanostructures emerged through helicene integration. Malinčík et. al. successfully synthesized the first helicene carbon nanostructure by integrating a [6]helicene unit into [7]CPP (Figure 1.13a).<sup>94</sup> This hybrid structure, named **[6,7]HPP** represents a combination where the [6]helicene endows the helicene carbon nanostructure with chirality and configurational stability typical for higher helicenes, while the radially conjugated seven paraphenylenes largely determine the optoelectronic properties. Characterization using XRD and NMR showed that the  $\pi$ -electron surface adopts a Möbius topology<sup>95</sup> that is, the  $\pi$ -electron

conjugation path is non-orientable in both solid state and in solution. Chirality transfer from the helicene unit to the CPP segment is evidenced by pronounced CD and CPL signals, with  $g_{lum}$  of about  $2.2 \times 10^{-3}$  comparable to [6]helicene ( $\sim 1 \times 10^{-3}$ ). Both CPL brightness and enantiomerization barrier are significantly better than for the standalone [6]helicene. Further research on helicene carbon nanohoops is presented in Chapter 4 and 5.

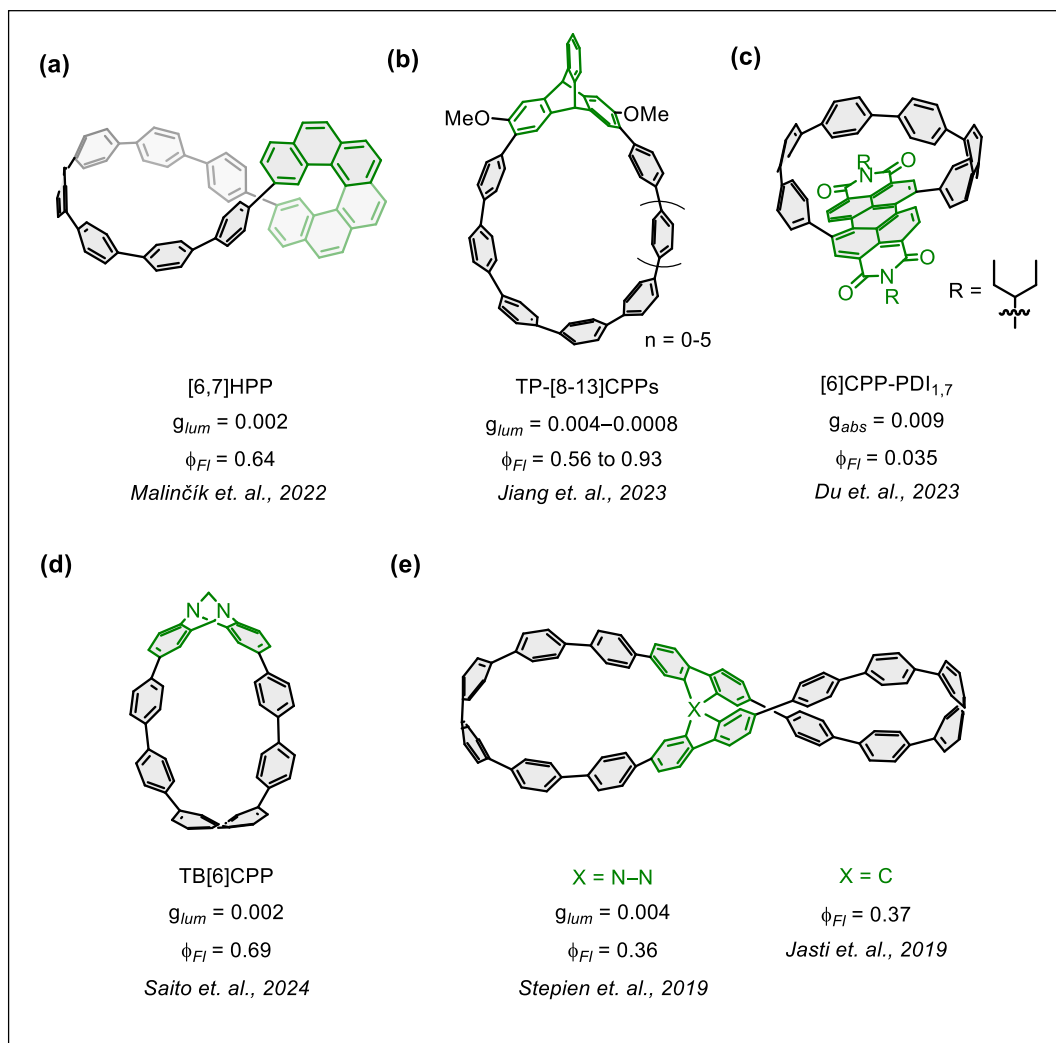


**Figure 1.13.** Chiral carbon nanohoops.<sup>94,96–99</sup>

Further, **TP-[n]CPPs**<sup>96</sup> ( $n=8-13$ , Figure 1.13b) have been achieved via symmetry breaking with a chiral triptycene motif, resulting in structures that display size-dependent emission with maxima red-shifting from 442 nm for **TP-[13]CPP** to 489 nm for **TP-[8]CPP**. The fluorescence quantum yields were determined to be from 92.9% for **TP-[13]CPP** to 56.1% for **TP-[8]CPP**, among the highest values reported for chiral nanohoops. The high fluorescence quantum yields are presumably attributed to the symmetry breaking, and the elevated radiative transition rates.

Chiroptical analysis revealed dissymmetry factors from  $3.52 \times 10^{-3}$  for TP-[8]CPP to  $0.81 \times 10^{-3}$  for TP-[13]CPP. The high brightness,  $B_{\text{CPL}}$  value was found to be 100.5 for TP-[11]CPP, which is among the highest among reported chiral nano hoops. Structural symmetry breaking can also be achieved by embedding achiral acceptor groups like perylene diimide (PDI) into the strained CPP framework (**[6]CPP-PDI<sub>1,7</sub>**) resulting in torsional distortion from the PDI, and pronounced chiroptical signals (Figure 1.13c).<sup>97</sup>

Tethering a stereogenic Troger's base (TB) to curved hexaparaphenylenes leads to a chiral nano hoop, **TB[6]CPP**, which possesses  $C_2$  symmetrical structure (Figure 1.13d).<sup>98</sup> The two stereogenic nitrogens with (*R,R*) and (*S,S*) configurations induce chiroptical activity in the nano hoop. This nano hoop exhibits pale blue emission with high quantum yield of approximately 0.69 and a dissymmetry factor of  $2.1 \times 10^{-3}$ . The stability of **TB[6]CPP** under acidic conditions was confirmed by experiments. While no racemization was observed upon heating a 1,2-dichloroethane solution of (*S,S*)-TB[6]CPP nano hoop and TFA at 65°C for 2 h, rapid racemization was observed upon heating a solution of (*S,S*)-TB with TFA at 65°C for 17 min. The remarkable stability of Troger's base in **TB[6]CPP** under acidic conditions can be attributed to the rigid macrocycle inhibiting the ring inversion process.

In recent years, chiral nano hoops research has also focused on the concept of topological chirality. Topologically chiral molecules require that their mirror image presentations are topologically distinct. A molecule must have a structure (a nonplanar molecular graph) that is non-superimposable on its mirror image, i.e., one cannot be converted into the other simply by stretching or deforming in 3D and bond cleavage is required for the transformation. Certain Möbius belts<sup>100,101</sup> and conjugated carbon nano hoops based on bicarbazole,<sup>99</sup> spirobifluorene<sup>102</sup> and PCP<sup>103</sup> possess this type of chirality. Such an approach has proven particularly successful in preserving the chiral integrity of macrocyclic systems, preventing racemization and enhancing their chiroptical performance. A noteworthy example is the report from Stepien and co-workers on lemniscular **[16]CPPL**, a radially conjugated carbon nano hoop (Figure 1.13e).<sup>99</sup> The strained nano hoop is sustained by a stereogenic element, namely, 9,9'-bicarbazole. Interestingly, the tight curvature in the lemniscate results in similar optical properties as smaller CPPs rather than non-twisted **[16]CPP**. The emission maxima for **[16]CPPL** is situated at 496 nm with  $\Phi_{\text{F}}$  of 0.36. The  $|g_{\text{lum}}|$  value was found to be  $3.7 \times 10^{-3}$  (498 nm) similar to the  $|g_{\text{abs}}|$  value of  $4.0 \times 10^{-3}$  implying a similarity in the ground state and excited state structure. A similar structure is reported by Jasti group, however, the chiroptical behavior was not investigated (Figure 1.13e).<sup>102</sup> Further research on topologically chiral nano hoops is presented in Chapter 2.

## 1.9 Discussion and Scope of the Thesis

As we learnt from the history of chirality and the fundamentals of CD and CPL, molecular handedness can profoundly influence optical and chiroptical properties of  $\pi$ -conjugated macrocycles. The discussion of molecular design principles for new CPL emitters reveals a persistent trade-off between  $g_{\text{lum}}$  and emission quantum yields. For instance, lanthanide complexes exhibit notably high  $g_{\text{lum}}$  but suffer from low emission efficiency, whereas SOMs provide bright emission but weak chiroptical dissymmetry. Bridging this gap remains a crucial challenge for advancing chiroptical research. Chiral carbon nano hoops emerge as promising platforms due to their curved architectures, rigid frameworks and tunable optoelectronic properties. However, their synthetic complexity, chemical instability and photophysical constraints pose significant hurdles. Moreover, achieving configurationally stable nano hoops with low racemization barriers is vital for effective enantiomeric resolution and detailed chiroptical studies. The impact of molecular strain on the chiroptical properties of carbon nano hoops is another underexplored aspect with potential to modulate chiroptical responses. Addressing these challenges, this thesis aims to develop rational molecular design strategies for bright, configurationally stable chiral carbon nano hoops that exhibit strong CPL, and study the effect of strain and curvature on both the photophysical and chiroptical properties of these systems.

The thesis is organized into the following chapters:

**Chapter 1** introduces the thesis by outlining the historical and conceptual foundations of chirality and its importance in chemistry and materials science. It highlights the role of key chiroptical spectroscopies, particularly circular dichroism and circularly polarized luminescence, as key tools for probing molecular handedness. The chapter then presents  $\pi$ -conjugated macrocycles, with a focus on cycloparaphenylenes ([n]CPPs), highlighting the unique properties and the synthetic challenges of bending benzene rings into strained nano hoops. Finally, it surveys strategies for introducing chirality into CPPs, setting the stage for the development of chiral nano hoops as potential circularly polarized light emitters explored in the following chapters.

**Chapter 2** presents the design, synthesis and characterization of chiral carbon nano hoops based on a planar-chiral pseudo-*meta*-[2,2]paracyclophane ([2.2]PCP) unit combined with a cycloparaphenylene (CPP) backbone. The work was expanded to develop a figure-eight,  $D_2$  symmetric nano hoop and further modified by introducing an electron-accepting benzothiadiazole (BTD) unit to probe structure–property relationships.

**Chapter 3** is dedicated to the synthesis, photophysical and systematic chiroptical investigation of carbon macrocycles that integrate pseudo *meta*-[2.2]paracyclophane unit which provides planar chirality, with a highly fluorescent benzothiadiazole (BTD) chromophore within a single, strained carbon nanohoop backbone. Photophysical characterization demonstrated the desired properties of the formed compounds, specifically achieving red-shifted fluorescence coupled with high fluorescence yields. The central goal is to use chiroptical techniques (CD and CPL) and theoretical calculations to define how exciton de(localization) influences the CPL performance, providing design guidelines towards balancing  $g_{\text{lum}}$  and  $\Phi_{\text{PL}}$ .

**Chapter 4** focuses on the synthesis and photophysical evaluation of  $\pi$ -extended chiral carbon nanohoos that incorporate [5]helicene into a [6]CPP backbone containing a highly fluorescence BTD unit as developed in Chapter 3. The primary objective is to investigate the effect of enhanced  $\pi$ -electron conjugation between the chiral unit and the emitting unit on the CPL properties. Chiral HPLC was used to resolve the enantiomers to measure the CD properties while CPL behaviour was predicted using computations.

**Chapter 5** expands on the concepts and synthesis developed in Chapter 4 and mainly investigates how strain influences the enantiomerization of [5]helicene in helicene carbon nanohoos. To systematically investigate this, a series of helicene carbon nanohoos ([5,*n*]HPPs), where *n* represents the number of phenylene rings, was synthesized and the enantiomerization barriers of individual hoops were experimentally determined using chiral HPLC. The results were theoretically validated.

**Chapter 6** serves as an outlook and focuses on a post-synthetic approach to increase strain in an already strained nanohoop featuring both a [5]helicene and a perylene diimide (PDI) unit through ring fusion via photocyclization. Spectroscopic and computational analysis are employed to reveal how  $\pi$ -extension contributes to strain buildup and modifies the photophysical properties of the strained nanohoop.

## 1.10 References

- (1) Biot, J.-B. Phénomènes de Polarisation Successive, Observés Dans Des Fluides Homogènes. *Bull. Sci. Par Société Philomatique* **1815**, 190–192.
- (2) Pasteur, L. Sur Les Relations Qui Peuvent Exister Entre La Forme Crystalline, La Composition Chimique et Le Sens de La Polarization Rotatoire. *Ann. Chim. Phys* **1848**, No. 24, 442–459.
- (3) Barron, L. D. On the Definition of Chirality. *Chem. – Eur. J.* **1996**, 2 (6), 743–744. <https://doi.org/10.1002/chem.19960020619>.
- (4) Le Bel, J. A. Sur Les Relations Qui Existent Entre Les Formules Atomiques Des Corps Organiques et Le Pouvoir Rotatoire de Leurs Dissolutions. *Bull. Société Chim. Paris* **22**, 337–347.
- (5) Van 't Hoff, J. H. Sur Les Formules de Structure Dans l'espace. *Arch. Néerl. Sci. Exactes Nat.* **1874**, 9, 445–454.
- (6) Meijer, E. W. Jacobus Henricus van 't Hoff; Hundred Years of Impact on Stereochemistry in the Netherlands. *Angew. Chem. Int. Ed.* **2001**, 40 (20), 3783–3789. [https://doi.org/10.1002/1521-3773\(20011015\)40:20%253C3783::AID-ANIE3783%253E3.0.CO;2-J](https://doi.org/10.1002/1521-3773(20011015)40:20%253C3783::AID-ANIE3783%253E3.0.CO;2-J).
- (7) Riddell, F. G.; Robinson, M. J. T. J. H. van't Hoff and J. A. Le Bel—Their Historical Context. *Tetrahedron* **1974**, 30 (13), 2001–2007. [https://doi.org/10.1016/S0040-4020\(01\)97330-2](https://doi.org/10.1016/S0040-4020(01)97330-2).
- (8) Kim, J. H.; Scialli, A. R. Thalidomide: The Tragedy of Birth Defects and the Effective Treatment of Disease. *Toxicol. Sci.* **2011**, 122 (1), 1–6. <https://doi.org/10.1093/toxsci/kfr088>.
- (9) Zhao, Q.; Peng, C.; Wang, Y.-T.; Zhan, G.; Han, B. Recent Progress on the Construction of Axial Chirality through Transition-Metal-Catalyzed Benzannulation. *Org. Chem. Front.* **2021**, 8 (11), 2772–2785. <https://doi.org/10.1039/D1QO00307K>.
- (10) López, R.; Palomo, C. Planar Chirality: A Mine for Catalysis and Structure Discovery. *Angew. Chem. Int. Ed.* **2022**, 61 (13), e202113504. <https://doi.org/10.1002/anie.202113504>.
- (11) Yang, H.; Feng, H.-X.; Zhou, L. Asymmetric Synthesis of Helicenes from Centrally Chiral Precursors. *Eur. J. Org. Chem.* **2024**, 27 (41), e202400671. <https://doi.org/10.1002/ejoc.202400671>.
- (12) Liu, M.; Zhang, L.; Wang, T. Supramolecular Chirality in Self-Assembled Systems. *Chem. Rev.* **2015**, 115 (15), 7304–7397. <https://doi.org/10.1021/cr500671p>.
- (13) Evans, N. H. Chiral Catenanes and Rotaxanes: Fundamentals and Emerging Applications. *Chem. – Eur. J.* **2018**, 24 (13), 3101–3112. <https://doi.org/10.1002/chem.201704149>.
- (14) Rickhaus, M.; Mayor, M.; Juriček, M. Chirality in Curved Polyaromatic Systems. *Chem Soc Rev* **2017**, 46 (6), 1643–1660. <https://doi.org/10.1039/C6CS00623J>.
- (15) Liu, T.; Huang, Y. Circularly Polarized Electroluminescence from Light-Emitting Diodes: Mechanisms, Materials, and Applications. *J. Mater. Chem. C* **2025**, 13 (35), 17996–18008. <https://doi.org/10.1039/D5TC02301G>.
- (16) Kitzmann, W. R.; Freudenthal, J.; Reponen, A.-P. M.; VanOrman, Z. A.; Feldmann, S. Fundamentals, Advances, and Artifacts in Circularly Polarized Luminescence (CPL) Spectroscopy. *Adv. Mater.* **2023**, 35 (44), 2302279. <https://doi.org/10.1002/adma.202302279>.
- (17) Andrews, D. L. *Photonics, Volume 1: Fundamentals of Photonics and Physics*; John Wiley & Sons, 2015.
- (18) *Circular Polarized Luminescence (The Basics)*. JASCO Inc. <https://jascoinc.com/learning-center/theory/spectroscopy/basics-of-circular-polarized-luminescence/> (accessed 2025-11-24).
- (19) Pescitelli, G.; Bari, L. D.; Berova, N. Conformational Aspects in the Studies of Organic Compounds by Electronic Circular Dichroism. *Chem. Soc. Rev.* **2011**, 40 (9), 4603–4625. <https://doi.org/10.1039/C1CS15036G>.
- (20) Castiglioni, E.; Abbate, S.; Lebon, F.; Longhi, G. Chiroptical Spectroscopic Techniques Based on Fluorescence. *Methods Appl. Fluoresc.* **2014**, 2 (2), 024006. <https://doi.org/10.1088/2050-6120/2/2/024006>.
- (21) Wang, Q.; Plum, E.; Yang, Q.; Zhang, X.; Xu, Q.; Xu, Y.; Han, J.; Zhang, W. Reflective Chiral Meta-Holography: Multiplexing Holograms for Circularly Polarized Waves. *Light Sci. Appl.* **2018**, 7 (1), 25. <https://doi.org/10.1038/s41377-018-0019-8>.
- (22) Schadt, M. Liquid Crystal Materials and Liquid Crystal Displays. *Annu. Rev. Mater. Res.* **1997**, 27 (Volume 27, 1997), 305–379. <https://doi.org/10.1146/annurev.matsci.27.1.305>.
- (23) Zhao, Y.; Niu, D.; Tan, J.; Jiang, Y.; Zhu, H.; Ouyang, G.; Liu, M. Alkaline-Earth Metal Ion Turn-On Circularly Polarized Luminescence and Encrypted Selective Recognition of AMP. *Small Methods* **2020**, 4 (10), 2000493. <https://doi.org/10.1002/smt.202000493>.
- (24) MacKenzie, L. E.; Pal, R. Circularly Polarized Lanthanide Luminescence for Advanced Security Inks. *Nat. Rev. Chem.* **2021**, 5 (2), 109–124. <https://doi.org/10.1038/s41570-020-00235-4>.
- (25) Sherson, J. F.; Krauter, H.; Olsson, R. K.; Julsgaard, B.; Hammerer, K.; Cirac, I.; Polzik, E. S. Quantum Teleportation between Light and Matter. *Nature* **2006**, 443 (7111), 557–560. <https://doi.org/10.1038/nature05136>.
- (26) Hassey, R.; Swain, E. J.; Hammer, N. I.; Venkataraman, D.; Barnes, M. D. Probing the Chiroptical Response of a Single Molecule. *Science* **2006**, 314 (5804), 1437–1439. <https://doi.org/10.1126/science.1134231>.

- (27) Farshchi, R.; Ramsteiner, M.; Herfort, J.; Tahraoui, A.; Grahn, H. T. Optical Communication of Spin Information between Light Emitting Diodes. *Appl. Phys. Lett.* **2011**, *98* (16), 162508. <https://doi.org/10.1063/1.3582917>.
- (28) Samoilov, B. N. Absorption and Luminescence Spectra of Uranyl Salts at Temperatures of Liquid Helium; Spektry Pogloshcheniya i Luminescentsii Uranilovykh Solei pri Temperature Zhidkogo Geliya. *Zhur Eksptl Teor. Fiz* **1948**, *18*, 1030–1040.
- (29) Emeis, C. A.; Oosterhoff, L. J. Emission of Circularly-Polarised Radiation by Optically-Active Compounds. *Chem. Phys. Lett.* **1967**, *1* (4), 129–132. [https://doi.org/10.1016/0009-2614\(67\)85007-3](https://doi.org/10.1016/0009-2614(67)85007-3).
- (30) Dekkers, H. P. J. M.; Closs, L. E. The Optical Activity of Low-Symmetry Ketones in Absorption and Emission. *J. Am. Chem. Soc.* **1976**, *98* (8), 2210–2219. <https://doi.org/10.1021/ja00424a034>.
- (31) Steinberg, I. Z.; Gafni, A. Sensitive Instrument for the Study of Circular Polarization of Luminescence. *Rev. Sci. Instrum.* **1972**, *43* (3), 409–413. <https://doi.org/10.1063/1.1685648>.
- (32) Richardson, F. S.; Riehl, J. P. Circularly Polarized Luminescence Spectroscopy. *Chem. Rev.* **1977**, *77* (6), 773–792. <https://doi.org/10.1021/cr60310a001>.
- (33) Luk, C. K.; Richardson, F. S. Circularly Polarized Luminescence Spectrum of Camphorquinone. *J. Am. Chem. Soc.* **1974**, *96* (7), 2006–2009. <https://doi.org/10.1021/ja00814a004>.
- (34) Riehl, J. P.; Richardson, F. S. Circularly Polarized Luminescence Spectroscopy. *Chem. Rev.* **1986**, *86* (1), 1–16. <https://doi.org/10.1021/cr00071a001>.
- (35) Wynberg, H.; Meijer, E. W.; Hummelen, J. C.; Dekkers, H. P. J. M.; Schippers, P. H.; Carlson, A. D. Circular Polarization Observed in Bioluminescence. *Nature* **1980**, *286* (5773), 641–642. <https://doi.org/10.1038/286641a0>.
- (36) Warnke, I.; Furche, F. Circular Dichroism: Electronic. *WIREs Comput. Mol. Sci.* **2012**, *2* (1), 150–166. <https://doi.org/10.1002/wcms.55>.
- (37) Rogers, D. M.; Jasim, S. B.; Dyer, N. T.; Auvray, F.; Réfrégiers, M.; Hirst, J. D. Electronic Circular Dichroism Spectroscopy of Proteins. *Chem* **2019**, *5* (11), 2751–2774. <https://doi.org/10.1016/j.chempr.2019.07.008>.
- (38) Chen, N.; Yan, B. Recent Theoretical and Experimental Progress in Circularly Polarized Luminescence of Small Organic Molecules. *Molecules* **2018**, *23* (12), 3376. <https://doi.org/10.3390/molecules23123376>.
- (39) Ma, K.; Chen, W.; Jiao, T.; Jin, X.; Sang, Y.; Yang, D.; Zhou, J.; Liu, M.; Duan, P. Boosting the Circularly Polarized Luminescence of Small Organic Molecules *via* Multi-Dimensional Morphology Control. *Chem. Sci.* **2019**, *10* (28), 6821–6827. <https://doi.org/10.1039/C9SC01577A>.
- (40) Arrico, L.; Di Bari, L.; Zinna, F. Quantifying the Overall Efficiency of Circularly Polarized Emitters. *Chem. – Eur. J.* **2021**, *27* (9), 2920–2934. <https://doi.org/10.1002/chem.202002791>.
- (41) Nagata, Y.; Mori, T. Irreverent Nature of Dissymmetry Factor and Quantum Yield in Circularly Polarized Luminescence of Small Organic Molecules. *Front. Chem.* **2020**, *8*. <https://doi.org/10.3389/fchem.2020.00448>.
- (42) Schippers, P. H.; Dekkers, H. P. J. M. Circular Polarization of Luminescence as a Probe for Intramolecular  $1n\pi^*$  Energy Transfer in Meso-Diketones. *J. Am. Chem. Soc.* **1983**, *105* (1), 145–146. <https://doi.org/10.1021/ja00339a041>.
- (43) Lunkley, J. L.; Shirotani, D.; Yamanari, K.; Kaizaki, S.; Muller, G. Extraordinary Circularly Polarized Luminescence Activity Exhibited by Cesium Tetrakis(3-Heptafluoro-Butylryl-(+)-Camphorato) Eu(III) Complexes in EtOH and CHCl<sub>3</sub> Solutions. *J. Am. Chem. Soc.* **2008**, *130* (42), 13814–13815. <https://doi.org/10.1021/ja805681w>.
- (44) Han, J.; Guo, S.; Lu, H.; Liu, S.; Zhao, Q.; Huang, W. Recent Progress on Circularly Polarized Luminescent Materials for Organic Optoelectronic Devices. *Adv. Opt. Mater.* **2018**, *6* (17), 1800538. <https://doi.org/10.1002/adom.201800538>.
- (45) Tanaka, H.; Ikenosako, M.; Kato, Y.; Fujiki, M.; Inoue, Y.; Mori, T. Symmetry-Based Rational Design for Boosting Chiroptical Responses. *Commun. Chem.* **2018**, *1* (1), 38. <https://doi.org/10.1038/s42004-018-0035-x>.
- (46) Hasegawa, M.; Nojima, Y.; Nagata, Y.; Usui, K.; Sugiura, K.; Mazaki, Y. Synthesis and Chiroptical Properties of Binaphthyl-Hinged [5]Helicenes. *Eur. J. Org. Chem.* **2023**, *26* (36), e202300656. <https://doi.org/10.1002/ejoc.202300656>.
- (47) Nojima, Y.; Hasegawa, M.; Hara, N.; Imai, Y.; Mazaki, Y. Small Figure-Eight Luminophores: Double-Twisted Tethered Cyclic Binaphthyls Boost Circularly Polarized Luminescence. *Chem. – Eur. J.* **2021**, *27* (19), 5923–5929. <https://doi.org/10.1002/chem.202005320>.
- (48) Kubo, H.; Shimizu, D.; Hirose, T.; Matsuda, K. Circularly Polarized Luminescence Designed from Molecular Orbitals: A Figure-Eight-Shaped [5]Helicene Dimer with D<sub>2</sub> Symmetry. *Org. Lett.* **2020**, *22* (23), 9276–9281. <https://doi.org/10.1021/acs.orglett.0c03506>.
- (49) Sato, S.; Yoshii, A.; Takahashi, S.; Furumi, S.; Takeuchi, M.; Isobe, H. Chiral Intertwined Spirals and Magnetic Transition Dipole Moments Dictated by Cylinder Helicity. *Proc. Natl. Acad. Sci.* **2017**, *114* (50), 13097–13101. <https://doi.org/10.1073/pnas.1717524114>.
- (50) Iijima, S. Helical Microtubules of Graphitic Carbon. *Nature* **1991**, *354* (6348), 56–58. <https://doi.org/10.1038/354056a0>.
- (51) Friederich, R.; Nieger, M.; Vögtle, F. Auf Dem Weg Zu Makrocyclischen Para-Phenylenen. *Chem. Ber.* **1993**, *126* (7), 1723–1732. <https://doi.org/10.1002/cber.19931260732>.

- (52) Jasti, R.; Bhattacharjee, J.; Neaton, J. B.; Bertozzi, C. R. Synthesis, Characterization, and Theory of [9]-, [12]-, and [18]Cycloparaphenylene: Carbon Nanohoop Structures. *J. Am. Chem. Soc.* **2008**, *130* (52), 17646–17647. <https://doi.org/10.1021/ja807126u>.
- (53) Takaba, H.; Omachi, H.; Yamamoto, Y.; Bouffard, J.; Itami, K. Selective Synthesis of [12]Cycloparaphenylene. *Angew. Chem. Int. Ed.* **2009**, *48* (33), 6112–6116. <https://doi.org/10.1002/anie.200902617>.
- (54) Yamago, S.; Watanabe, Y.; Iwamoto, T. Synthesis of [8]Cycloparaphenylene from a Square-Shaped Tetranuclear Platinum Complex. *Angew. Chem.* **2010**, *122* (4), 769–771. <https://doi.org/10.1002/ange.200905659>.
- (55) Darzi, E. R.; Jasti, R. The Dynamic, Size-Dependent Properties of [5]–[12]Cycloparaphenylenes. *Chem. Soc. Rev.* **2015**, *44* (18), 6401–6410. <https://doi.org/10.1039/C5CS00143A>.
- (56) Golder, M. R.; Jasti, R. Syntheses of the Smallest Carbon Nanohoos and the Emergence of Unique Physical Phenomena. *Acc. Chem. Res.* **2015**, *48* (3), 557–566. <https://doi.org/10.1021/ar5004253>.
- (57) Segawa, Y.; Fukazawa, A.; Matsuura, S.; Omachi, H.; Yamaguchi, S.; Irle, S.; Itami, K. Combined Experimental and Theoretical Studies on the Photophysical Properties of Cycloparaphenylenes. *Org. Biomol. Chem.* **2012**, *10* (30), 5979–5984. <https://doi.org/10.1039/C2OB25199J>.
- (58) Fujitsuka, M.; Cho, D. W.; Iwamoto, T.; Yamago, S.; Majima, T. Size-Dependent Fluorescence Properties of [n]Cycloparaphenylenes (n = 8–13), Hoop-Shaped  $\pi$ -Conjugated Molecules. *Phys. Chem. Chem. Phys.* **2012**, *14* (42), 14585–14588. <https://doi.org/10.1039/C2CP42712E>.
- (59) Segawa, Y.; Omachi, H.; Itami, K. Theoretical Studies on the Structures and Strain Energies of Cycloparaphenylenes. *Org. Lett.* **2010**, *12* (10), 2262–2265. <https://doi.org/10.1021/ol1006168>.
- (60) Adamska, L.; Nayyar, I.; Chen, H.; Swan, A. K.; Oldani, N.; Fernandez-Alberti, S.; Golder, M. R.; Jasti, R.; Doorn, S. K.; Tretiak, S. Self-Trapping of Excitons, Violation of Condon Approximation, and Efficient Fluorescence in Conjugated Cycloparaphenylenes. *Nano Lett.* **2014**, *14* (11), 6539–6546. <https://doi.org/10.1021/nl503133e>.
- (61) Reddy, V. S.; Camacho, C.; Xia, J.; Jasti, R.; Irle, S. Quantum Dynamics Simulations Reveal Vibronic Effects on the Optical Properties of [n]Cycloparaphenylenes. *J. Chem. Theory Comput.* **2014**, *10* (9), 4025–4036. <https://doi.org/10.1021/ct500524y>.
- (62) Nishihara, T.; Segawa, Y.; Itami, K.; Kanemitsu, Y. Excited States in Cycloparaphenylenes: Dependence of Optical Properties on Ring Length. *J. Phys. Chem. Lett.* **2012**, *3* (21), 3125–3128. <https://doi.org/10.1021/jz3014826>.
- (63) Camacho, C.; Niehaus, T. A.; Itami, K.; Irle, S. Origin of the Size-Dependent Fluorescence Blueshift in [n]Cycloparaphenylenes. *Chem. Sci.* **2012**, *4* (1), 187–195. <https://doi.org/10.1039/C2SC20878D>.
- (64) Nishihara, T.; Segawa, Y.; Itami, K.; Kanemitsu, Y. Exciton Recombination Dynamics in Nanoring Cycloparaphenylenes. *Chem. Sci.* **2014**, *5* (6), 2293–2296. <https://doi.org/10.1039/C3SC53462F>.
- (65) Sundholm, D.; Taubert, S.; Pichierri, F. Calculation of Absorption and Emission Spectra of [n]Cycloparaphenylenes: The Reason for the Large Stokes Shift. *Phys. Chem. Chem. Phys.* **2010**, *12* (11), 2751–2757. <https://doi.org/10.1039/B922175A>.
- (66) Nijegorodov, N. I.; Downey, W. S.; Danailov, M. B. Systematic Investigation of Absorption, Fluorescence and Laser Properties of Some *p*- and *m*-Oligophenylenes. *Spectrochim. Acta. A. Mol. Biomol. Spectrosc.* **2000**, *56* (4), 783–795. [https://doi.org/10.1016/S1386-1425\(99\)00167-5](https://doi.org/10.1016/S1386-1425(99)00167-5).
- (67) Banerjee, M.; Shukla, R.; Rathore, R. Synthesis, Optical, and Electronic Properties of Soluble Poly-*p*-Phenylene Oligomers as Models for Molecular Wires. *J. Am. Chem. Soc.* **2009**, *131* (5), 1780–1786. <https://doi.org/10.1021/ja805102d>.
- (68) Lovell, T. C.; Colwell, C. E.; Zakharov, L. N.; Jasti, R. Symmetry Breaking and the Turn-on Fluorescence of Small, Highly Strained Carbon Nanohoos. *Chem. Sci.* **2019**, *10* (13), 3786–3790. <https://doi.org/10.1039/C9SC00169G>.
- (69) Hermann, M.; Wassy, D.; Esser, B. Conjugated Nanohoos Incorporating Donor, Acceptor, Hetero- or Polycyclic Aromatics. *Angew. Chem. Int. Ed Engl.* **2021**, *60* (29), 15743–15766. <https://doi.org/10.1002/anie.202007024>.
- (70) Lovell, T. C.; Fosnacht, K. G.; Colwell, C. E.; Jasti, R. Effect of Curvature and Placement of Donor and Acceptor Units in Cycloparaphenylenes: A Computational Study. *Chem. Sci.* **2020**, *11* (44), 12029–12035. <https://doi.org/10.1039/D0SC03923C>.
- (71) Kuwabara, T.; Orii, J.; Segawa, Y.; Itami, K. Curved Oligophenylenes as Donors in Shape-Persistent Donor–Acceptor Macrocycles with Solvatochromic Properties. *Angew. Chem. Int. Ed.* **2015**, *54* (33), 9646–9649. <https://doi.org/10.1002/anie.201503397>.
- (72) Darzi, E. R.; Hirst, E. S.; Weber, C. D.; Zakharov, L. N.; Lonergan, M. C.; Jasti, R. Synthesis, Properties, and Design Principles of Donor–Acceptor Nanohoos. *ACS Cent. Sci.* **2015**, *1* (6), 335–342. <https://doi.org/10.1021/acscentsci.5b00269>.
- (73) Lovell, T. C.; Garrison, Z. R.; Jasti, R. Synthesis, Characterization, and Computational Investigation of Bright Orange-Emitting Benzothiadiazole [10]Cycloparaphenylene. *Angew. Chem. Int. Ed.* **2020**, *59* (34), 14363–14367. <https://doi.org/10.1002/anie.202006350>.

- (74) Qiu, Z.-L.; Tang, C.; Wang, X.-R.; Ju, Y.-Y.; Chu, K.-S.; Deng, Z.-Y.; Hou, H.; Liu, Y.-M.; Tan, Y.-Z. Tetra-Benzothiadiazole-Based [12]Cycloparaphenylene with Bright Emission and Its Supramolecular Assembly. *Angew. Chem.* **2020**, *132* (47), 21054–21058. <https://doi.org/10.1002/ange.202008505>.
- (75) Kayahara, E.; Zhai, X.; Yamago, S. Synthesis and Physical Properties of [4]Cyclo-3,7-Dibenzo[b,d]Thiophene and Its S,S-Dioxide. *Can. J. Chem.* **2017**, *95* (4), 351–356. <https://doi.org/10.1139/cjc-2016-0474>.
- (76) Li, S.; Aljhdli, M.; Thakellapalli, H.; Farajidizaji, B.; Zhang, Y.; Akhmedov, N. G.; Milsman, C.; Popp, B. V.; Wang, K. K. Synthesis and Structure of a Functionalized [9]Cycloparaphenylene Bearing Three Indeno[2,1-a]Fluorene-11,12-Dione-2,9-Diyl Units. *Org. Lett.* **2017**, *19* (15), 4078–4081. <https://doi.org/10.1021/acs.orglett.7b01866>.
- (77) Ball, M.; Zhong, Y.; Fowler, B.; Zhang, B.; Li, P.; Etkin, G.; Paley, D. W.; Decatur, J.; Dalsania, A. K.; Li, H.; Xiao, S.; Ng, F.; Steigerwald, M. L.; Nuckolls, C. Macrocyclization in the Design of Organic N-Type Electronic Materials. *J. Am. Chem. Soc.* **2016**, *138* (39), 12861–12867. <https://doi.org/10.1021/jacs.6b05474>.
- (78) Ito, H.; Mitamura, Y.; Segawa, Y.; Itami, K. Thiophene-Based, Radial  $\pi$ -Conjugation: Synthesis, Structure, and Photophysical Properties of Cyclo-1,4-Phenylene-2,5'-Thienylenes. *Angew. Chem. Int. Ed.* **2015**, *54* (1), 159–163. <https://doi.org/10.1002/anie.201409389>.
- (79) Thakellapalli, H.; Farajidizaji, B.; Butcher, T. W.; Akhmedov, N. G.; Popp, B. V.; Petersen, J. L.; Wang, K. K. Syntheses and Structures of Thiophene-Containing Cycloparaphenylenes and Related Carbon Nano-hoops. *Org. Lett.* **2015**, *17* (14), 3470–3473. <https://doi.org/10.1021/acs.orglett.5b01514>.
- (80) Farajidizaji, B.; Thakellapalli, H.; Li, S.; Huang, C.; Baughman, N. N.; Akhmedov, N. G.; Popp, B. V.; Petersen, J. L.; Wang, K. K. Synthesis of Cycloparaphenylenes Bearing Furan-2,5-Diyl or 2,2'-Bifuran-5,5'-Diyl Units in the Macrocyclic Structures. *Chem. – Eur. J.* **2016**, *22* (46), 16420–16424. <https://doi.org/10.1002/chem.201604036>.
- (81) Myśliwiec, D.; Kondratowicz, M.; Lis, T.; Chmielewski, P. J.; Stepień, M. Highly Strained Nonclassical Nanotube End-Caps. A Single-Step Solution Synthesis from Strain-Free, Non-Macrocyclic Precursors. *J. Am. Chem. Soc.* **2015**, *137* (4), 1643–1649. <https://doi.org/10.1021/ja511951x>.
- (82) Kuroda, Y.; Sakamoto, Y.; Suzuki, T.; Kayahara, E.; Yamago, S. Tetracyclo(2,7-Carbazole): Diatropicity and Paratropicity of Inner Regions of Nano-hoops. *J. Org. Chem.* **2016**, *81* (8), 3356–3363. <https://doi.org/10.1021/acs.joc.6b00425>.
- (83) Lucas, F.; Sicard, L.; Jeannin, O.; Rault-Berthelot, J.; Jacques, E.; Quinton, C.; Poriol, C. [4]Cyclo-N-Ethyl-2,7-Carbazole: Synthesis, Structural, Electronic and Charge Transport Properties. *Chem. – Eur. J.* **2019**, *25* (32), 7740–7748. <https://doi.org/10.1002/chem.201901066>.
- (84) Tran-Van, A.-F.; Wegner, H. A. Nano-Rings with a Handle – Synthesis of Substituted Cycloparaphenylenes. *Beilstein J. Nanotechnol.* **2014**, *5* (1), 1320–1333. <https://doi.org/10.3762/bjnano.5.145>.
- (85) Yagi, A.; Segawa, Y.; Itami, K. Synthesis and Properties of [9]Cyclo-1,4-Naphthylene: A  $\pi$ -Extended Carbon Nanoring. *J. Am. Chem. Soc.* **2012**, *134* (6), 2962–2965. <https://doi.org/10.1021/ja300001g>.
- (86) Povie, G.; Segawa, Y.; Nishihara, T.; Miyauchi, Y.; Itami, K. Synthesis and Size-Dependent Properties of [12], [16], and [24]Carbon Nanobelts. *J. Am. Chem. Soc.* **2018**, *140* (31), 10054–10059. <https://doi.org/10.1021/jacs.8b06842>.
- (87) Kręćjasz, R. B.; Malinčík, J.; Šolomek, T. Exploring Silyl Protecting Groups for the Synthesis of Carbon Nano-hoops. *Synthesis* **2023**, *55* (9), 1355–1366. <https://doi.org/10.1055/a-2008-9505>.
- (88) Sisto, T. J.; Zakharov, L. N.; White, B. M.; Jasti, R. Towards  $\pi$ -Extended Cycloparaphenylenes as Seeds for CNT Growth: Investigating Strain Relieving Ring-Openings and Rearrangements. *Chem. Sci.* **2016**, *7* (6), 3681–3688. <https://doi.org/10.1039/C5SC04218F>.
- (89) Wassy, D.; Hermann, M.; Wössner, J. S.; Frédéric, L.; Pieters, G.; Esser, B. Enantiopure Nano-hoops through Racemic Resolution of Diketo[n]CPPs by Chiral Derivatization as Precursors to DBP[n]CPPs. *Chem. Sci.* **2021**, *12* (30), 10150–10158. <https://doi.org/10.1039/D1SC02718B>.
- (90) Omachi, H.; Segawa, Y.; Itami, K. Synthesis and Racemization Process of Chiral Carbon Nanorings: A Step toward the Chemical Synthesis of Chiral Carbon Nanotubes. *Org. Lett.* **2011**, *13* (9), 2480–2483. <https://doi.org/10.1021/ol200730m>.
- (91) Wang, J.; Zhuang, G.; Chen, M.; Lu, D.; Li, Z.; Huang, Q.; Jia, H.; Cui, S.; Shao, X.; Yang, S.; Du, P. Selective Synthesis of Conjugated Chiral Macrocycles: Sidewall Segments of (-)/(+)-(12,4) Carbon Nanotubes with Strong Circularly Polarized Luminescence. *Angew. Chem. Int. Ed.* **2020**, *59* (4), 1619–1626. <https://doi.org/10.1002/anie.201909401>.
- (92) Wang, J.; Shi, H.; Wang, S.; Zhang, X.; Fang, P.; Zhou, Y.; Zhuang, G.-L.; Shao, X.; Du, P. Tuning the (Chir)Optical Properties and Squeezing out the Inherent Chirality in Polyphenylene-Locked Helical Carbon Nanorings. *Chem. – Eur. J.* **2022**, *28* (13), e202103828. <https://doi.org/10.1002/chem.202103828>.
- (93) Sato, K.; Hasegawa, M.; Nojima, Y.; Hara, N.; Nishiuchi, T.; Imai, Y.; Mazaki, Y. Circularly Polarized Luminescence of a Stereogenic Curved Paraphenylene Anchoring a Chiral Binaphthyl in Solution and Solid State. *Chem. – Eur. J.* **2021**, *27* (4), 1323–1329. <https://doi.org/10.1002/chem.202004283>.
- (94) Malinčík, J.; Gaikwad, S.; Mora-Fuentes, J. P.; Boillat, M.-A.; Prescimone, A.; Häussinger, D.; Campaña, A. G.; Šolomek, T. Circularly Polarized Luminescence in a Möbius Helicene Carbon Nano-hoop. *Angew. Chem. Int. Ed.* **2022**, *61* (37), e202208591. <https://doi.org/10.1002/anie.202208591>.

- (95) Malinčik, J.; Šolomek, T. Topological Bistability of the  $\pi$ -System in a Helicene Carbon Nanohoop. *Synlett* **2024**, *35* (15), 1739–1744. <https://doi.org/10.1055/a-2223-7245>.
- (96) Guo, S.; Liu, L.; Li, X.; Liu, G.; Fan, Y.; He, J.; Lian, Z.; Yang, H.; Chen, X.; Jiang, H. Highly Luminescent Chiral Carbon Nanohoos via Symmetry Breaking with a Triptycene Unit: Bright Circularly Polarized Luminescence and Size-Dependent Properties. *Small* **2024**, *20* (14), 2308429. <https://doi.org/10.1002/sml.202308429>.
- (97) Li, A.; Zhang, X.; Wang, S.; Wei, K.; Du, P. Synthesis and Physical Properties of a Perylene Diimide-Embedded Chiral Conjugated Macrocyclic. *Org. Lett.* **2023**, *25* (7), 1183–1187. <https://doi.org/10.1021/acs.orglett.3c00152>.
- (98) Yoshigoe, Y.; Shimada, H.; Takaki, T.; Imai, Y.; Saito, S. Synthesis and Isolation of a Homochiral Nanohoop Composed of a Tröger's Base and Hexaparaphenylene. *Chem. – Eur. J.* **2024**, *30* (16), e202304059. <https://doi.org/10.1002/chem.202304059>.
- (99) Senthilkumar, K.; Kondratowicz, M.; Lis, T.; Chmielewski, P. J.; Cybińska, J.; Zafra, J. L.; Casado, J.; Vives, T.; Crassous, J.; Favereau, L.; Stępień, M. Lemniscular [16]Cycloparaphenylene: A Radially Conjugated Figure-Eight Aromatic Molecule. *J. Am. Chem. Soc.* **2019**, *141* (18), 7421–7427. <https://doi.org/10.1021/jacs.9b01797>.
- (100) Schaller, G. R.; Topić, F.; Rissanen, K.; Okamoto, Y.; Shen, J.; Herges, R. Design and Synthesis of the First Triply Twisted Möbius Annulene. *Nat. Chem.* **2014**, *6* (7), 608–613. <https://doi.org/10.1038/nchem.1955>.
- (101) Fan, W.; Fukunaga, T. M.; Wu, S.; Han, Y.; Zhou, Q.; Wang, J.; Li, Z.; Hou, X.; Wei, H.; Ni, Y.; Isobe, H.; Wu, J. Synthesis and Chiral Resolution of a Triply Twisted Möbius Carbon Nanobelt. *Nat. Synth.* **2023**, *2* (9), 880–887. <https://doi.org/10.1038/s44160-023-00317-3>.
- (102) Schaub, T. A.; Prantl, E. A.; Kohn, J.; Bursch, M.; Marshall, C. R.; Leonhardt, E. J.; Lovell, T. C.; Zakharov, L. N.; Brozek, C. K.; Waldvogel, S. R.; Grimme, S.; Jasti, R. Exploration of the Solid-State Sorption Properties of Shape-Persistent Macrocyclic Nanocarbons as Bulk Materials and Small Aggregates. *J. Am. Chem. Soc.* **2020**, *142* (19), 8763–8775. <https://doi.org/10.1021/jacs.0c01117>.
- (103) He, J.; Yu, M.-H.; Lian, Z.; Fan, Y.-Q.; Guo, S.-Z.; Li, X.-N.; Wang, Y.; Wang, W.-G.; Cheng, Z.-Y.; Jiang, H. Lemniscular Carbon Nanohoos with Contiguous Conjugation from Planar Chiral [2.2]Paracyclophane: Influence of the Regioselective Synthesis on Topological Chirality. *Chem. Sci.* **2023**, *14* (16), 4426–4433. <https://doi.org/10.1039/D2SC06825G>.